Li *et al. Biochar* (2026) 8:114
https://doi.org/10.1007/s42773-026-00635-7

Biochar

ORIGINAL RESEARCH Open Access

Reduction in N_2O and NH_3 emissions with combined use of dual inhibitors and biochar in a tea field soil in subtropical central China

Yuefeng Li[1], Yanyan Li[1], Haifeng Zhang[1], Qiyuan Liao[1], Huixiu Zhan[1], Chengli Tong[1], Yong Li[2], Jinshui Wu[1] and Jianlin Shen[1*]

Abstract

Excessive nitrogen (N) fertilization in tea plantations often leads to substantial nitrous oxide (N_2O) emissions, which exacerbate global warming, and to pronounced ammonia (NH_3) volatilization, which is closely associated with air pollution and aquatic eutrophication. Although N transformation inhibitors and biochar have shown promise in mitigating these gaseous losses, their combined effects and the underlying mechanisms in tea fields remain poorly understood. A 2-year field experiment was conducted in a subtropical hilly tea plantation to evaluate the individual and combined effects of dual inhibitors (the urease inhibitor N-(*n*-butyl) thiophosphoric triamide, NBPT, and the nitrification inhibitor 3,4-dimethylpyrazole phosphate, DMPP) and biochar (28 t ha^{-1}) on N_2O and NH_3 emissions. Four treatments were established: conventional N fertilization (CON), N fertilizer amended with dual inhibitors (NI), N fertilizer combined with both biochar and dual inhibitors (BNI), and a zero-N control (CK). The results showed that the CON treatment produced high cumulative gaseous emissions (N_2O: 25.8 kg ha^{-1}; NH_3: 75.8 kg ha^{-1}). The NI treatment reduced the N_2O and NH_3 emission factors by 54.5% and 20.0%, respectively, while the BNI treatment achieved comparable mitigation efficiencies (49.8% for N_2O and 20.2% for NH_3). Both treatments significantly suppressed the abundance of key N-cycling functional genes, including ammonia-oxidizing bacteria (AOB) and the nitrite reductase gene (*nirS*), with NI exerting a stronger inhibitory effect on AOB. Gaseous emissions originated predominantly from the tea rows rather than from the inter-row ridges. Structural equation modeling (SEM) and random forest (RF) analyses revealed that the mitigation effect was driven by shifts in soil N transformation dynamics and substrate availability. Specifically, NBPT significantly reduced short-term soil NH_4^+–N concentrations following fertilization, thereby decreasing substrate availability for NH_3 volatilization, whereas DMPP significantly suppressed the abundance of key N-cycling functional genes, particularly AOB and *nirS*, thereby inhibiting nitrification-driven N_2O production. Additionally, the BNI treatment increased the tea yield by 6.7% and plant N uptake by 14.4%. In conclusion, applying dual inhibitors, either alone or in combination with biochar, effectively mitigates N_2O and NH_3 emissions while maintaining tea productivity offering a practical strategy for environmentally sustainable tea cultivation.

Highlights

- Conventional fertilization caused high N_2O and NH_3 emissions from tea plantations.
- Applying dual inhibitors alone or with biochar reduced N_2O and NH_3 emission factors by up to 50% and 20%.

*Correspondence:
Jianlin Shen
jlshen@isa.ac.cn
Full list of author information is available at the end of the article

© The Author(s) 2026. **Open Access** This article is licensed under a Creative Commons Attribution 4.0 International License, which permits use, sharing, adaptation, distribution and reproduction in any medium or format, as long as you give appropriate credit to the original author(s) and the source, provide a link to the Creative Commons licence, and indicate if changes were made. The images or other third party material in this article are included in the article's Creative Commons licence, unless indicated otherwise in a credit line to the material. If material is not included in the article's Creative Commons licence and your intended use is not permitted by statutory regulation or exceeds the permitted use, you will need to obtain permission directly from the copyright holder. To view a copy of this licence, visit http://creativecommons.org/licenses/by/4.0/.

Springer

- Combining inhibitors with biochar increased tea yield by 6.7% and N uptake by 14.4%.
- N emissions were cut by suppressing soil NO_3^-–N, altering NH_4^+–N transformation dynamics, and key microbial genes.

Keywords N cycling, Biochar, Urease and nitrification inhibitors, Flux monitoring, Functional gene

Graphical Abstract

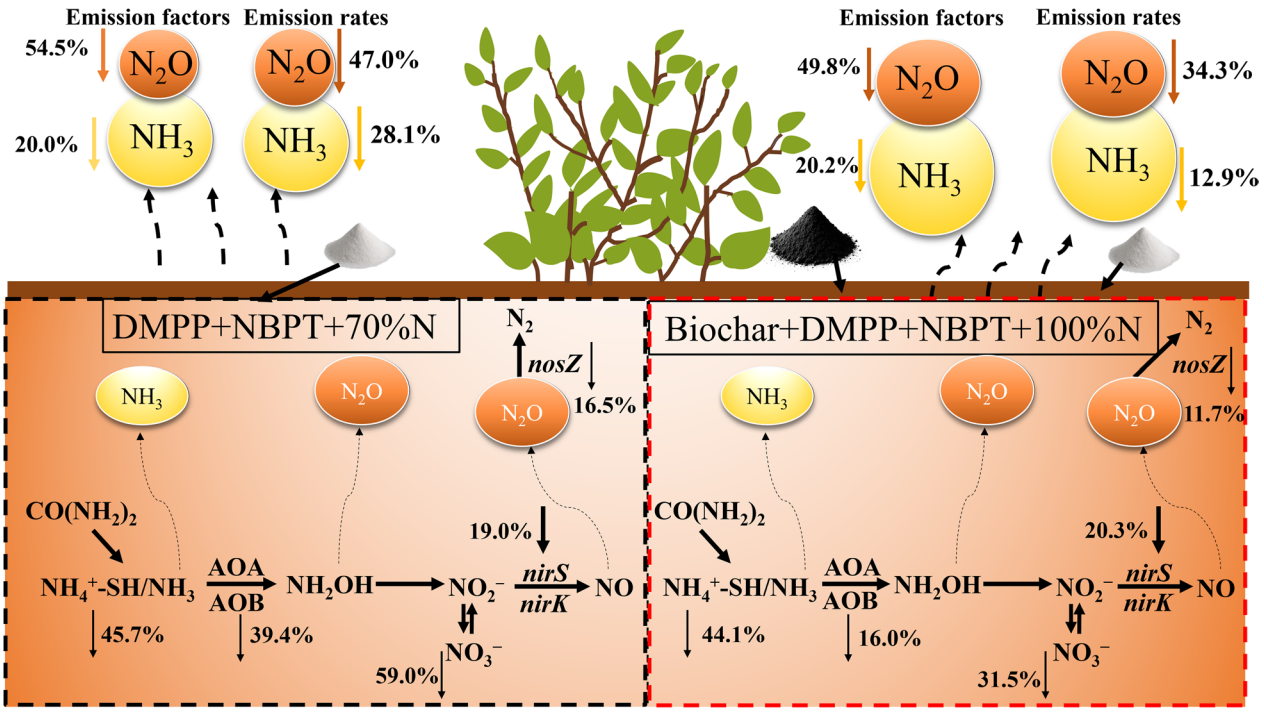

1 Introduction

Tea (*Camellia sinensis* L.) is the most widely consumed beverage globally, and its substantial economic and social value has led to its cultivation in an increasing number of countries. Tea is commercially grown in 62 countries, with China accounting for approximately 61% of the global tea-growing area (FAO 2018). In tea plantations across China, nitrogen (N) fertilizer application rates can be as high as 500–2600 kg ha^{-1} per growing season to sustain high yields (Shen et al. 2022).

The average N application rate in major tea-producing regions of China is 444 kg ha^{-1} yr^{-1} (Zou et al. 2021), which far exceeds the global average N application rate of 95–118 kg ha^{-1} yr^{-1} for cereal crops (Smerald et al. 2023). Tea plantations are a major global source of nitrous oxide (N_2O), with annual emissions ranging from 0.02 to 38.54 kg ha^{-1} yr^{-1} (Han et al. 2023a, b). Ammonia (NH_3) volatilization is another major pathway of reactive N loss in tea plantation systems. NH_3 is a well-documented precursor of fine particulate matter ($PM_{2.5}$) and a major source of indirect N_2O emissions (Song et al. 2024). Furthermore, NH_3 deposition drives ecosystem acidification and eutrophication via atmospheric reactive N deposition (Uwiragiye et al. 2024), a process largely driven by excessive N fertilizer application (Yi et al. 2025). Optimizing the synchrony between N supply and crop N demand is essential for developing evidence-based N management strategies in tea plantation systems. Such optimization can simultaneously improve nitrogen use efficiency (NUE), sustain crop productivity, and mitigate concurrent N_2O and NH_3 emissions.

Various field management strategies have been developed to mitigate reactive N losses, mainly in the form of N_2O emissions and NH_3 volatilization, while sustaining optimal crop productivity. These strategies include the use of dual inhibitors (nitrification and urease inhibitors)

(He et al. 2022; Wang et al. 2023a, b), biochar soil amendment (Wang et al. 2024), and optimization of N fertilizer application rates (Ju et al. 2009). Collectively, these agronomic practices improve agricultural NUE while maintaining stable crop yields (Li et al. 2023a, b). Urease inhibitors (UIs) retard the hydrolysis of urea into ammonium (NH_4^+), thereby reducing NH_4^+ concentrations in the soil solution and the associated risk of NH_3 volatilization (Qi et al. 2022). In contrast, nitrification inhibitors (NIs) act by suppressing the nitrification process mediated by ammonia-oxidizing bacteria (AOB) and ammonia-oxidizing archaea (AOA). This inhibitory effect blocks the enzymatic oxidation of NH_4^+ to hydroxylamine, which is then oxidized to nitrite (NO_2^-) and subsequently to nitrate (NO_3^-). This action directly limits the substrate availability for N_2O production via nitrification, and indirectly suppresses N_2O emissions by reducing the nitrate (NO_3^-–N) pool available for denitrification (Han et al. 2023a, b; Elrys et al. 2023). However, the use of NIs alone can prolong the retention of mineral N as NH_4^+–N in soil, thereby increasing the risk of NH_3 volatilization (Cui et al. 2025; Zhu et al. 2021). Therefore, the combined application of urea and nitrification inhibitors (i.e., dual inhibitors) represents a promising agronomic strategy for concurrently mitigating N_2O and NH_3 emissions. A combination of N-(*n*-butyl) thiophosphoric triamide (NBPT) and 3,4-dimethylpyrazole phosphate (DMPP) was selected for this study due to its high adaptability to subtropical hilly tea plantation ecosystems. First, NBPT exhibits excellent thermal and moisture stability, enabling it to maintain effective urease inhibition under the warm, humid conditions typical of subtropical tea plantations. This, in turn, slows urea hydrolysis, thereby directly mitigating the risk of NH_3 volatilization (Chen et al. 2019a, b; Shen et al. 2022). Second, DMPP is particularly well-suited to acidic soils, where it effectively suppresses ammonia oxidation and subsequent nitrification. This inhibition prolongs the retention of NH_4^+–N in the soil matrix and reduces substrate availability for N_2O production (Li et al. 2023a, b; He et al. 2022). Third, the combined use of these two inhibitors produces synergistic and complementary effects: it alleviates the risk of NH_4^+–N accumulation associated with DMPP alone, while compensating for the inability of NBPT alone to suppress nitrification. Consequently, this synergy enables the simultaneous mitigation of NH_3 and N_2O emissions. The mitigation efficacy of dual-inhibitor application is influenced by multiple factors, including soil physicochemical properties, climatic conditions, and field management practices (Hao et al. 2023; Wang et al. 2025). To date, the mitigation effects of dual inhibitors on N_2O and NH_3 emissions from tea plantations in China's subtropical hilly regions remain largely unquantified.

Biochar is a porous, alkaline, carbonaceous material produced by the pyrolysis of biomass under oxygen-limited conditions (Hu et al. 2024). It is characterized by a high recalcitrant organic carbon content, large specific surface area, and strong adsorption capacity (Wu et al. 2021). Biochar amendment is widely regarded as a promising strategy for agricultural soil management because it delivers dual benefits: improving soil fertility and mitigating greenhouse gas (GHG) emissions (Ngaba et al. 2026). However, the effects of biochar on soil NH_3 volatilization and N_2O emissions remain highly variable and context-dependent, posing a major challenge for large-scale field applications. Previous studies have reported contrasting effects of biochar amendment on reactive N gas emissions from soil. A substantial body of literature supports the GHG mitigation potential of biochar. For instance, Fungo et al. (2019) and Park et al. (2019) observed significant reductions in both NH_3 and N_2O emissions following biochar application, which were attributed to the suppression of ammonification, enhanced gaseous adsorption, and promotion of complete denitrification to dinitrogen (N_2). Wu et al. (2019) reported a pronounced reduction in NH_3 volatilization from straw biochar-amended soils with no significant effect on N_2O emissions, which was primarily attributed to the strong adsorptive retention of inorganic N by biochar. Zhong et al. (2025) demonstrated that biochar amendment reduces N_2O emissions by enhancing soil N immobilization and pH buffering. Conversely, the stimulation of N_2O emissions by biochar amendment has also been widely reported. Deng et al. (2019) observed that fruit-shell-derived biochar consistently increased N_2O emissions in acidic soils from *Camellia oleifera* plantations across different N forms, accompanied by an elevated temperature sensitivity of N_2O production. This considerable heterogeneity in biochar performance is primarily attributed to three categories of driving factors: soil and climatic conditions (e.g., soil texture, pH, and organic matter content), the intrinsic properties of biochar, and field agronomic management practices (Wang et al. 2019; He et al. 2024). Biochar can directly modulate the rate and direction of soil N transformation by altering the abundance, diversity, and community structure of N-cycling functional microorganisms. Song et al. (2014) reported that biochar amendment significantly altered the community composition of ammonia oxidizers and nitrification dynamics in alkaline coastal soils, processes central to regulating reactive N losses in soil. Second, the interaction between biochar and N-loss mitigation additives introduces additional uncertainty. Biochar can adsorb nitrification inhibitor molecules, thereby attenuating their inhibitory efficacy on N_2O emissions (Pokharel and Chang 2021); this is a non-negligible factor

when the two amendments are co-applied in field practices. To date, most studies on biochar and N inhibitors have focused on their individual effects on gaseous reactive N loss and crop yield in cereal cropping systems, such as wheat and rice monocultures. However, intensively managed tea plantations, characterized by excessive N input, long-term soil acidification, and unique rhizosphere biogeochemical processes, differ substantially from annual cereal cropping systems. The combined effects of dual inhibitors and biochar on NH_3 and N_2O emissions, tea yield, and the underlying interactive mechanisms in tea plantation systems remain largely unquantified. This critical knowledge gap limits the development of low-carbon, high-efficiency N-management strategies for tea plantations.

In this study, two hypotheses were proposed: (a) the combined application of urease inhibitor and nitrification inhibitor would reduce both NH_3 volatilization and N_2O emissions in acidic tea plantation soils and (b) the co-application of these dual inhibitors with biochar would modulate their mitigation efficacy on NH_3 volatilization and N_2O emissions, owing to the potential adsorption of inhibitor molecules by biochar and concomitant changes in soil properties (e.g., soil mineral N contents as well as soil N-cycling microbial abundances). To test these hypotheses, a 2-year field experiment was conducted in a typical subtropical hilly tea plantation in southern China. This study aimed to (1) quantify the effects of dual inhibitors and their combination with biochar on NH_3 and N_2O emissions, and (2) elucidate the underlying mechanisms.

2 Methods and materials

2.1 Site description and experimental design

This study was conducted at the Changsha Agro-Environmental Observation and Research Station in Jinjing Town, Changsha City, Hunan Province, China. The experimental site was a 16-year-old tea plantation, where the tea plants had a canopy width of 0.8 m, a height of 1.0 m, and a row spacing of 0.5 m. The region has a mid-subtropical monsoon climate with a mean annual temperature of 17.5 °C and annual precipitation of 1390 mm (data automatically collected by an on-site meteorological station ~10 m from the experimental plots from 2010 to 2024). Approximately 70% of the annual precipitation falls between April and June. During the 2022–2024 experimental period, daily precipitation ranged from 0 to 96.0 mm. Specifically, in the 2022–2023 growing season, precipitation was concentrated from May to August, totaling 1153.4 mm, whereas in the 2023–2024 growing season, precipitation was concentrated from April to June, totaling 1377.3 mm. In contrast, precipitation was relatively low from September to February in both seasons (Fig. 1). Daily air temperature during the experimental period ranged from −11.1 to 32.8 °C. The mean soil temperature during the tea-growing season was 19.0 °C in 2022–2023 and 18.5 °C in 2023–2024. Soil moisture and temperature were automatically monitored every 30 min using TH5 sensors (Beijing Tanghua Technology Co., Ltd, China). The sensors were installed vertically at depths of 5 and 10 cm in the conventional N fertilization (CON) plots. The mean values from the two depths were used for subsequent analyses; these depths were chosen to avoid interference from the tea root zone. The soil is classified as red soil (Ultisol; USDA Soil Taxonomy), derived from highly weathered granite, and is similar to the soils in adjacent Masson pine forests and tea plantations in the region (Wu et al. 2016).

The observation period of this study covered the period from May 2022 to April 2024. The total experimental area was 672 m^2 and consisted of four treatments, each with three biological replicates. Each treatment block averaged 168 m^2, and each plot averaged 56 m^2. Each plot contained three tea rows, and one sampling point was established in the inter-row ridge. This location was chosen primarily because it was less affected by the experimental treatments and therefore showed minimal treatment-induced variation. The materials used were as follows: N fertilizers (urea, at 450 kg N ha^{-1}, and locally sourced rapeseed cake organic fertilizer, at 150 kg N ha^{-1}, co-applied); phosphorus fertilizer (single superphosphate applied at 68 kg P ha^{-1}); dual nitrification and urease inhibitors (DMPP and NBPT, each applied at 1% of the total N application rate); and biochar (supplied by Hubei Jinri Ecological Energy Co., Ltd, derived from rice straw pyrolyzed at 500 °C, applied at 28 t ha^{-1} and incorporated into the 0–20 cm soil layer, equivalent to 1% of the soil mass). The physicochemical properties of the biochar, rapeseed cake, and initial soil are presented in Table S1. The four treatments were as follows. (1) CK (zero N control): no fertilizer was applied. (2) CON: N applied at the local conventional rate. (3) NI (reduced N input with dual inhibitors): 70% of the conventional N rate, supplemented with the dual inhibitors NBPT and DMPP, which was designed to test whether optimized N management could reduce gaseous N loss while increasing tea yield and plant N uptake. (4) BNI (biochar amendment with dual inhibitors): the biochar amendment described above was applied together with the dual inhibitors NBPT and DMPP (He et al. 2018).

Detailed fertilizer application rates for each treatment are provided in Table S2. Field management practices were as follows: The dual inhibitors were mixed uniformly with urea and rapeseed cake organic fertilizer before field application. Urea was split-applied in April (300 kg N ha^{-1}) and September (150 kg N ha^{-1}) for both the 2022–2023 and 2023–2024 tea-growing

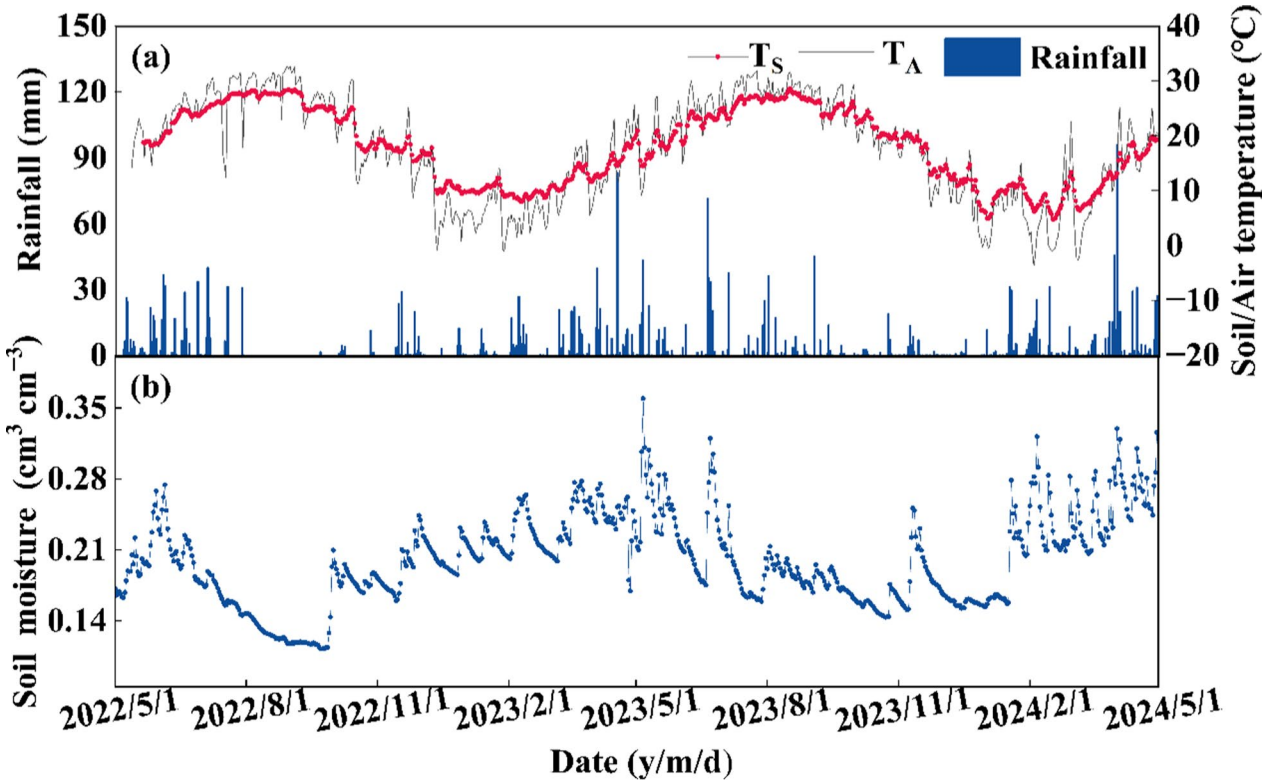

Fig. 1 The daily dynamics of rainfall, air temperature (T_A), soil temperature (T_S), and soil moisture (SM, volumetric water content) over the 2022–2024 period at the study site. (**a**) Rainfall, T_A, and T_S; (**b**) SM

seasons. Organic rapeseed cake fertilizer was applied each December during the experimental period. Phosphorus fertilizer (single superphosphate) was applied annually in April using the same banding method as the N fertilizer and was placed in trenches on one side of the tea ridges at a soil depth of 10–15 cm, followed by immediate backfilling with soil to minimize gaseous N losses. Owing to the drought conditions from August to October 2022, four supplemental irrigation events were conducted, supplying a total of 539.4 m^3 ha^{-1}, to maintain normal tea plant growth. All other agronomic management practices followed local conventional tea farming standards. Cumulative N_2O and NH_3 emissions were calculated using a weighted average method to quantify total gaseous N emissions from the tea plantation system.

To elucidate the underlying microscale mechanisms of NH_3 mitigation by the dual inhibitors observed in the field experiment, a laboratory incubation experiment was conducted under controlled constant-temperature conditions using the same tea plantation soil and identical inhibitor application rates as those in the field experiment. Full details of the experimental design, analytical methods, and corresponding results are provided in the Supplementary Materials.

2.2 Field measurements of soil N_2O and NH_3 fluxes

Soil N_2O fluxes were measured using the static chamber-gas chromatography. In each plot, stainless-steel chamber bases were permanently inserted to a soil depth of 20 cm. Chambers deployed in tea rows had a base area of 0.36 m^2 (0.9 m × 0.4 m) and a height of 0.4 m; those in inter-row ridges had a base area of 0.64 m^2 (0.8 m × 0.8 m) and a height of 1 m, and each enclosed one tea plant during sampling. The exterior of each chamber was wrapped with foam insulation to minimize internal temperature fluctuations caused by solar radiation. Gas samples were collected weekly between 09:00 and 11:00. Before each sampling, the chamber lid was secured to the base and sealed using a water-filled groove. Two small 12-V fans were mounted inside each chamber to ensure homogeneous mixing of the headspace gas. Over a 40-min chamber closure period, four gas samples were collected at equal intervals using a 30-mL syringe and immediately injected into 12-mL pre-evacuated vials. The headspace air temperature was recorded during sampling with a thermometer (JM624, China). All gas samples were analyzed within 2 weeks of collection using a gas chromatograph (Agilent 7890D, Agilent Technologies, USA). High-purity N_2 was used as the carrier gas, and the chromatographic column temperature was maintained at 55 °C. The N_2O

concentrations were quantified using an electron capture detector (ECD). A mixture of CO_2 and N_2 (1:9, v/v) was used as the detector makeup gas to minimize CO_2 interference in N_2O quantification.

NH_3 volatilization was measured using a dynamic chamber coupled with intermittent air extraction. NH_3 emissions were monitored simultaneously from both tea rows and inter-row ridges. Dynamic sampling chambers were positioned at the center of the tea rows and beneath the tea plants in the inter-row ridges. Each cylindrical dynamic chamber had an internal diameter of 20 cm, and the internal air exchange rate was maintained at 15–20 air exchanges per min. Volatilized NH_3 from the chamber headspace was drawn by an air-extraction pump through an absorption bottle containing 0.1 L of 0.05 mol L^{-1} dilute H_2SO_4 solution. The NH_3 volatilization flux and cumulative emissions were subsequently calculated. Following each fertilization event, NH_3 volatilization was sampled daily for 7 consecutive days, with two sampling sessions per day (09:00–11:00 and 15:00–17:00 local time). The NH_3 concentration in the absorption solution was quantified using a continuous-flow autoanalyzer (SEAL Analytical, Germany).

2.2.1 N_2O flux calculation

The N_2O flux (F, mg N m^{-2} h^{-1}) was calculated as follows:

$$F = \frac{M}{V_0} \times H \times \frac{P}{P_0} \times \frac{T_0}{T} \times \frac{d_c}{d_t} \tag{1}$$

The molar mass of the target gas is represented by M in g mol^{-1}; V_0 refers to the molar volume under standard conditions of 22.4 L mol^{-1}; H denotes the height, in meter, from the floor of the stationary box to the top of the air chamber; P_0 and T_0 represent the standard atmospheric pressure (101.3 kPa) and temperature (273.15 K), respectively; P denotes the atmospheric pressure within the chamber at the time of sampling, and $\frac{P}{P_0}$ denotes the pressure correction factor; T represents the air temperature inside the chamber at the time of sampling, and $\frac{T_0}{T}$ represents the temperature correction factor; and $\frac{d_c}{d_t}$ denotes the gradient of the target gas concentration (ppb h^{-1}) during the observation period after sealing (He et al. 2022).

The cumulative soil N_2O emissions from tea plantations were calculated as follows:

$$E_C = \left(\frac{f_1 + f_n}{2} + \sum_{i=1}^{n-1} \frac{(f_{i+1} + f_i) \times (t_{i+1} - t_i)}{2} \right) \times 24 \times \frac{365}{t_i - t_1} \times \frac{10000}{1000 \times 1000 \times 1000} \tag{2}$$

In the formula, the variable E_C denotes the cumulative soil N_2O emissions (kg N ha^{-1}); f_1 and f_n denotes the emission flux of the target gas at the first and last samplings, respectively; f_i and f_{i+1} denotes the emission flux of the target gas at the second and third samplings (mg N m^{-2} h^{-1}), respectively; and t_{i+1} and t_i denote the time intervals between the first and second samplings (days), respectively.

The direct emission factor (EF) of N_2O from tea plantations was calculated using the following equation:

$$EF_{N_2O} = \frac{E_F - E_0}{N} \tag{3}$$

EF_{N_2O} refers to the rate of N fertilizer loss due to N_2O emissions. E_F and E_0 represent the total N_2O emissions (kg ha^{-1}) for treatments with and without N, respectively, and N represents the amount of N applied during the observation period (kg ha^{-1}).

2.2.2 NH_3 volatilization

The NH_3 flux was calculated using the following formula.

$$F = C \times V \times 10^{-3} \times 10^{-6} \times \frac{10^4}{\pi \times r^2} \times 6 \tag{4}$$

The NH_3 flux (kg N ha^{-1} d^{-1}) is represented by F; the concentration of NH_4^+–N in the absorbing solution (mg L^{-1}) is represented by C; the volume of dilute H_2SO_4 absorbing solution (mL) is represented by V; the aforementioned conversion factor, mass conversion factor, and area conversion factor, are represented by 10^{-3}, 10^{-6} and 10^4; respectively; the radius of the gas chamber (m) is represented by r; and 6 denotes the time conversion factor, which is the ratio of 24 h to the ammonia volatilization collection time of 4 h (Chen et al. 2019a, b).

Cumulative emissions were calculated as follows:

$$F_C = \left[\frac{F_1 + F_n}{2} + \sum_{i=1}^{n} \left(\frac{F_i + F_{i+1}}{2} \right) \times (t_{i+1} - t_i) \right] \tag{5}$$

Cumulative emissions of NH_3 (kg N ha^{-1}) are represented by the symbol F_C. The emission fluxes at the first and last samplings are represented by F_1 and F_n, respectively, and those at any two consecutive samplings are represented by F_i and F_{i+1} (kg N ha^{-1} d^{-1}). The number of observations per season is represented by n. The time interval between two consecutive samplings (d) is represented by $t_{i+1} - t_i$.

The NH_3 EF was calculated as follows:

$$EF_{NH_3} = \frac{F_x - F_0}{Q} \quad (6)$$

EF_{NH_3} indicates the rate of NH_3 volatilization loss (%); F_x and F_0 are the NH_3 volatilization fluxes (kg N ha^{-1}) for the N fertilizer application and no N fertilizer application treatments, respectively; and Q is the amount of N applied (kg N ha^{-1}).

The global warming potential (GWP) arising from N_2O and NH_3 emissions was calculated as:

$$GWP = \left[298\left(E_{N_2O} + 0.01E_{NH_3}\right) \times \frac{44}{28}\right]/1000 \quad (7)$$

In the calculations of N_2O and NH_3, 298 is defined as the GWP of N_2O over a 100-year time horizon relative to that of CO_2, indicating that N_2O has 298 times the warming potential of CO_2. E_{N_2O} and E_{NH_3} are the cumulative emissions of N_2O and NH_3, respectively, are in kg ha^{-1}. In addition, 0.01 was set as the conversion factor to account for the fact that 1% of deposited NH_3 was converted to N_2O during the calculation.

2.2.3 Net environmental economic benefit (NEEB)

The NEEB was evaluated as follows:

$$NEEB_i = (Y_i \times P) - C_{i,plot} - \left(E_{N_2O,i,plot} \times EC_{N_2O} + E_{NH_3,i,plot} \times EC_{NH_3}\right) \quad (8)$$

$NEEB_i$ refers to the net environmental-economic benefit of treatment, expressed in Chinese Yuan per hectare per year (CNY ha^{-1} yr^{-1}). Here, i denotes the experimental treatment; Y_i is the tea yield for treatment i (unit: kg); P is the market price of dry tea; $C_{i,\,plot}$ is the total production input cost for treatment i per plot; $E_{N_2O,i,plot}$ indicates the cumulative N_2O emission for treatment i per plot (unit: kg N ha^{-1}); EC_{N_2O} is the mitigation cost for the greenhouse effect induced by N_2O; $E_{NH_3,i,plot}$ is the cumulative NH_3 emission for treatment i per plot (unit: kg N ha^{-1}); and EC_{NH_3} is the mitigation cost for atmospheric pollution caused by NH_3 (Cai et al. 2023).

2.3 Soil and plant sampling and analysis

Soil samples for chemical analysis were collected at weekly to biweekly intervals during the fertilizer application period from May 2022 to April 2024. In each tea row, five soil cores were collected in an 'S' pattern using a stainless-steel auger (3.8 cm diameter) and composited into a single composite sample per row. Additional soil samples were collected from each tea row concurrently with each gas-sampling event. After removing stones and visible plant residues, the samples were stored at 4 °C prior to analysis for NH_4^+–N, NO_3^-–N, and dissolved organic carbon (DOC). Soil NH_4^+–N and NO_3^-–N were extracted from fresh soil samples sieved to <2 mm using 2 mol L^{-1} K_2SO_4 solution, and quantified using an AA3 continuous flow auto-analyzer (Seal Analytical, Norderstedt, Germany) (Chen et al. 2019a, b). DOC was quantified using a total organic carbon (TOC) analyzer (TOC-VWP, Shimadzu, Japan). For microbial functional gene analysis, soil samples were collected seasonally over the 2022–2023 experimental cycle on August 28, 2022 (summer, pre-fertilization), October 24, 2022 (autumn), December 30, 2022 (winter), and May 2, 2023 (spring, post-fertilization). The collected soil samples were sieved to <2 mm, thoroughly homogenized, and stored at −80 °C pending molecular analysis. Microbial molecular analysis quantified the absolute abundance of functional genes for AOB, AOA, and denitrifying gene (*nirK*, *nirS*, and *nosZ*). Detailed primer sequences and qPCR amplification conditions are listed in Table S3. Detailed protocols for soil DNA extraction and qPCR analysis are provided in the Supplementary Materials.

At the tea harvest, the fresh tea yield of each experimental plot was recorded. The moisture contents of the collected tea plant samples were determined by standard oven-drying. The dried tea plant samples were ground and sieved to pass a 0.15-mm sieve for total nitrogen (TN) analysis. For TN determination, the dried samples were digested with concentrated H_2SO_4 in the presence of a catalyst mixture (K_2SO_4, $CuSO_4$, and Se). The N concentration in the resulting digest was quantified using a flow-injection auto-analyzer (FIAstar 5000, Foss Tecator, Sweden) (Bao 2000).

2.4 Net environmental economic benefit

The unit price of bulk green tea was set at 96.6 CNY kg^{-1}. This price was derived from a field survey conducted by Xu et al. (2021) across 105 tea plantations and 80 tea-processing factories in Shengzhou, Zhejiang Province, a core green tea-producing region of China. The aforementioned study by Xu et al. (2021) targeted the domestic mass market for bulk green tea and estimated a refining-stage revenue of 14–18 CNY kg^{-1}. This estimation was based on a total refining cost of 49.84 CNY kg^{-1} and an industry-average profit margin of 20–30%. Using the 2017 average annual exchange rate of 6.9 CNY USD^{-1}, the lower bound of this revenue range (14 CNY kg^{-1}) was converted, yielding the adopted unit price of 96.6 CNY kg^{-1}. This unit price was adopted in the present study because the study region has a subtropical monsoon climate similar to that of Shengzhou.

Furthermore, soils in both regions are characteristically acidic and well-suited to bulk green tea

production, with no significant differences in tea quality or agronomic characteristics reported between the two regions. The mitigation costs for greenhouse gas damage driven by N_2O emissions and atmospheric pollution from NH_3 volatilization were set at 160 and 65 CNY kg^{-1} N, respectively, following Cai et al. (2023). The market prices of agricultural production inputs used in this study were as follows: rapeseed cake organic fertilizer, at 4 CNY kg^{-1}; urea, at 6 CNY kg^{-1}; calcium magnesium phosphate fertilizer, at 1 CNY kg^{-1}; biochar, at 2600 CNY t^{-1}; and the dual inhibitors DMPP and NBPT, each at 100 CNY kg^{-1}.

2.5 Data analysis and statistics

All statistical analyses were performed using R software (version 4.5.2; R Core Team, 2025). One-way ANOVA followed by Duncan's multiple range test (DMRT) was performed using the 'agricolae' package to identify significant differences ($P < 0.05$) among treatments for variables, including soil physicochemical properties, tea yield, plant N uptake, cumulative N_2O and NH_3 emissions, and their EFs. Random forest (RF) modeling and structural equation modeling (SEM) were performed using the 'randomForest' and 'lavaan' packages, respectively, to quantify the effects of environmental factors on N_2O and NH_3 emissions and elucidate their direct and indirect driving pathways. Prior to SEM analysis, multicollinearity among key numerical variables (e.g., NH_4^+–N, NO_3^-–N, soil moisture, and microbial gene abundances) was assessed using variance inflation factors (VIFs), with a preset threshold of VIF < 5 to exclude severe multicollinearity and ensure compliance with SEM modeling assumptions. Model fit was assessed using standard goodness-of-fit indices: the comparative fit index (CFI > 0.90), Tucker–Lewis index (TLI > 0.90), root mean square error of approximation (RMSEA < 0.05), standardized root mean square residual (SRMR < 0.08), and a non-significant chi-square (χ^2) ($P > 0.05$). Data on soil physicochemical properties, dynamic N_2O and NH_3 emissions, and tea yield were processed and visualized in Origin 2024. The relationship between N_2O and NH_3 emissions was analyzed using linear regression.

3 Results

3.1 N_2O and NH_3 emission fluxes

Over the entire 2-year observation period, N_2O fluxes in the CK plots ranged from 0.0 to 0.19 kg N ha^{-1} d^{-1}, with an average daily flux of 0.02 kg N ha^{-1} d^{-1} (Fig. 2a). Peak N_2O fluxes occurred in May immediately after chemical N fertilizer application, with maximum values of 0.83, 0.27, and 0.27 kg N ha^{-1} d^{-1} for the CON, NI, and BNI treatments, respectively. In comparison, peak N_2O fluxes following organic fertilizer application were 0.49, 0.15, and 0.15 kg N ha^{-1} d^{-1} for the CON, NI, and BNI treatments, respectively. Regarding NH_3 volatilization fluxes, consistent with the patterns observed for N_2O, the maximum emission fluxes after chemical N fertilizer application occurred in May for the CON treatment (6.69 kg N ha^{-1} d^{-1}), while the peak fluxes for the CK, NI, and BNI treatments were recorded in October (0.52, 2.76, and 3.71 kg N ha^{-1} d^{-1}, respectively). In contrast, peak NH_3 fluxes occurred following organic fertilizer application in March for the CK (0.21 kg N ha^{-1} d^{-1}) and NI (0.63 kg N ha^{-1} d^{-1}) treatments, in December for the CON treatment (2.06 kg N ha^{-1} d^{-1}), and in April for the BNI treatment (1.03 kg N ha^{-1} d^{-1}) (Fig. 2b).

Overall, both NH_3 volatilization and N_2O emission fluxes were consistently lower in the inter-row ridges than in the tea rows over the entire observation period. For N_2O fluxes in the inter-row ridges, peak fluxes occurred in June for the CK treatment (0.09 kg N ha^{-1} d^{-1}), March for CON (0.09 kg N ha^{-1} d^{-1}), April for NI (0.11 kg N ha^{-1} d^{-1}), and May for BNI (0.14 kg N ha^{-1} d^{-1}). The mean daily N_2O fluxes for the four treatments were 0.02, 0.01, 0.03, and 0.03 kg N ha^{-1} d^{-1}, respectively (Fig. 2c). In contrast to the staggered peak timing observed for N_2O fluxes, peak NH_3 volatilization fluxes in the inter-row ridges for the CK, CON, NI, and BNI treatments all occurred in October, with maximum values of 0.36, 2.84, 1.10, and 1.71 kg N ha^{-1} d^{-1}, respectively (Fig. 2d).

3.2 Cumulative N_2O and NH_3 emissions, GWP, and emission factors

Significant positive correlations were observed between the gaseous N emissions and N application rates across all treatments throughout the observation period. Overall, all N-fertilizer treatments produced significantly higher

(See figure on next page.)

Fig. 2 Daily dynamics of N_2O and NH_3 fluxes from the tea rows and inter-row ridges across treatments during the 2022–2024 growing season. **a** N_2O fluxes in the tea rows; **b** NH_3 fluxes in the tea rows; **c** N_2O fluxes in the inter-row ridges; **d** NH_3 fluxes in the inter-row ridges. The treatments were CK (blank control), CON (conventional fertilization), NI (dual inhibitors treatment), and BNI (biochar combined with dual inhibitors treatment). Arrows denote the timing of fertilizer application: black arrows mark the application of chemical fertilizer, while red arrows mark the application of rapeseed cake fertilizer. Error bars represent the standard error of three replicates ($n = 3$)

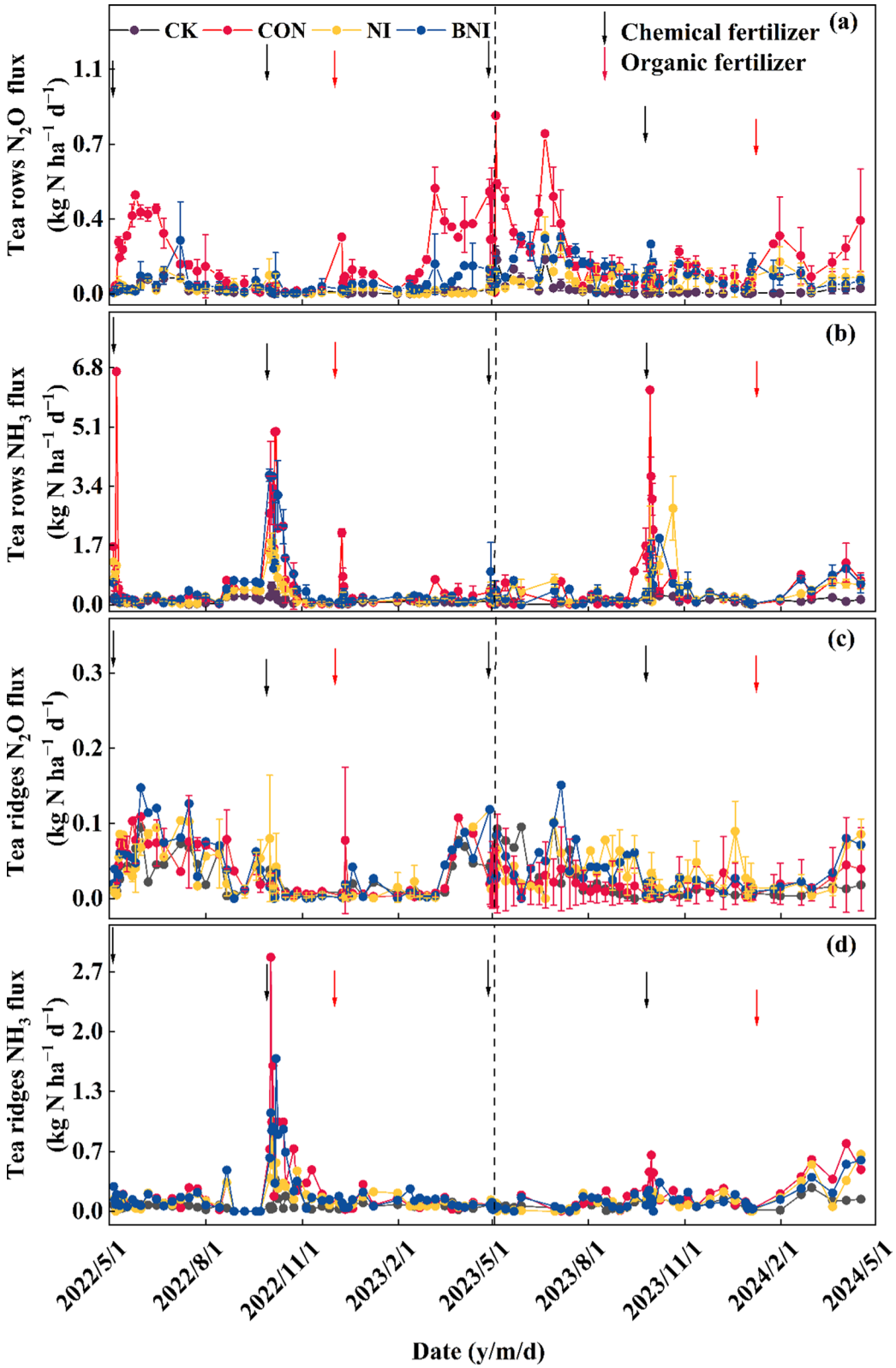

Fig. 2 (See legend on previous page.)

cumulative gaseous N emissions than the CK treatment. In the first experimental year (2022–2023), cumulative N_2O emissions were 8.5, 22.1, 10.6, and 14.2 kg ha^{-1} for the CK, CON, NI, and BNI treatments, respectively (Table 1). Compared with the CON treatment, the NI and BNI treatments significantly reduced N_2O emissions by 51.8% and 35.7%, respectively ($P<0.05$). In the second experimental year (2023–2024), cumulative N_2O emissions were 7.5, 29.5, 16.7, and 19.7 kg ha^{-1} for the CK, CON, NI, and BNI treatments, respectively. Compared with the CON treatment, the NI and BNI treatments significantly reduced N_2O emissions by 43.4% and 33.3%, respectively ($P<0.05$). Across the entire 2-year experimental period (2022–2024), cumulative N_2O emissions were 16.0, 51.5, 27.3, and 33.8 kg ha^{-1} for the CK, CON, NI, and BNI treatments, respectively. Compared with the CON treatment, the NI and BNI treatments significantly reduced total N_2O emissions by 47.0% and 34.3%, respectively ($P<0.05$). Notably, the NI treatment achieved a significantly greater N_2O mitigation effect than the BNI treatment ($P<0.05$). Cumulative NH_3 volatilization showed a similar trend to that of cumulative N_2O emissions, with both the NI and BNI treatments achieving significant mitigation effects. However, the NH_3 mitigation efficiencies of both treatments were lower than the corresponding N_2O mitigation efficiencies, especially for the BNI treatment. In the second experimental year (2023–2024), cumulative NH_3 volatilization was 31.6, 80.8, 59.8, and 64.8 kg ha^{-1} for the CK, CON, NI, and BNI treatments, respectively (Table 1). Relative to the CON treatment, the NI and BNI treatments significantly reduced NH_3 volatilization by 26.0% and 19.8%, respectively ($P<0.05$). Across the entire 2-year experimental period, cumulative NH_3 volatilization was 54.8, 151.6, 109.0, and 132.1 kg ha^{-1} for the CK, CON, NI, and BNI treatments, respectively. Compared with the CON treatment, the NI and BNI treatments significantly reduced the total NH_3 volatilization by 28.1% and 12.9%, respectively ($P<0.05$).

GWP in the first experimental year (2022–2023) was 4.1, 10.7, 5.2, and 7.0 t CO_2-eq ha^{-1} for the CK, CON, NI, and BNI treatments, respectively. Compared with the CON treatment, the NI and BNI treatments significantly reduced GWP by 51.1% and 34.8%, respectively ($P<0.05$). Consistent with the first-year trends, similar GWP patterns were observed in the second experimental year (2023–2024) (Table 1), with the NI and BNI treatments achieving GWP reductions of 42.9% and 32.9%, respectively. Compared with the CON treatment, the NI and BNI treatments exhibited significantly lower EFs for both N_2O emissions and NH_3 volatilization. In the first experimental year, the N_2O EFs were 2.3% (CON), 0.5% (NI), and 1.0% (BNI), corresponding to significant reductions of 77.5% (NI) and 58.1% (BNI) relative to the CON treatment ($P<0.05$). In the second experimental year, the N_2O EFs were 3.7%, 2.2%, and 2.0% for the CON, NI, and BNI treatments, respectively; this gave significant reductions of 40.3% for NI and 44.7% for BNI, relative to the CON treatment (Table 1). In the first experimental year, the NH_3 volatilization EFs for the CON, NI, and BNI treatments were 8.0%, 6.2%, and 7.4%, respectively. The NI and BNI treatments achieved significant reductions

Table 1 Average cumulative gaseous N emissions, GWP, emission factors, and NEEB for 2022–2023, 2023–2024, and for the 2-year experimental period

Year	Treatment	N losses (kg N ha^{-1})		GWP (t CO_2-eq ha^{-1})	EF (%)		NEEB (CNY ha^{-1} yr^{-1})
		N_2O	NH_3		N_2O	NH_3	
2022–2023	CK	8.5 ± 0.1d	23.2 ± 0.2d	4.1 ± 0.07d	–	–	–
	CON	22.1 ± 0.9a	70.9 ± 1.3a	10.7 ± 0.4a	2.3 ± 0.2a	8.0 ± 0.2a	–
	NI	10.6 ± 0.4c	49.2 ± 0.4c	5.2 ± 0.2c	0.5 ± 0.09c	6.2 ± 0.09c	–
	BNI	14.2 ± 1.4b	67.4 ± 0.4b	7.0 ± 0.6b	1.0 ± 0.2b	7.4 ± 0.07b	–
2023–2024	CK	7.5 ± 0.2d	31.6 ± 0.1d	3.7 ± 0.1d	–	–	–
	CON	29.5 ± 1.8a	80.8 ± 1.4a	14.2 ± 0.8a	3.7 ± 0.3a	8.2 ± 0.2a	–
	NI	16.7 ± 1.4c	59.8 ± 1.3c	8.1 ± 0.6c	2.2 ± 0.3b	6.7 ± 0.3b	–
	BNI	19.7 ± 0.1b	64.8 ± 0.8b	9.5 ± 0.05b	2.0 ± 0.02b	5.5 ± 0.1c	–
Two-year average	CK	8.0 ± 0.2d	27.4 ± 0.2d	3.9 ± 0.07d	–	–	103,749.6 ± 5358.5b
	CON	25.8 ± 1.1a	75.8 ± 1.3a	12.4 ± 0.5a	3.0 ± 0.2a	8.1 ± 0.2a	49,134.7 ± 5410.8c
	NI	13.7 ± 0.5c	54.5 ± 0.5c	6.7 ± 0.2c	1.4 ± 0.1b	6.5 ± 0.1b	100,510.8 ± 7432.0b
	BNI	16.9 ± 0.6b	66.1 ± 0.4b	8.2 ± 0.3b	1.5 ± 0.1b	6.4 ± 0.06b	116,301.8 ± 871.2a

CK blank control, *CON* conventional fertilization, *NI* dual inhibitor treatment, *BNI* biochar combined with dual inhibitor treatment, *GWP* global warming potential, *EF* emission factor, *NEEB* net environmental economic benefit (CNY ha^{-1} yr^{-1}), *CO_2-eq* CO_2 equivalent

Different lowercase letters in the same column indicate significant differences among treatments according to Duncan's multiple range test ($P<0.05$)

of 21.9% and 7.3%, respectively, compared with the CON treatment ($P < 0.05$). In the second experimental year, the NH_3 volatilization EFs for the NI and BNI treatments were significantly reduced by 18.2% and 32.6%, respectively, relative to the CON treatment ($P < 0.05$). Across the entire 2-year experimental period, the 2-year mean N_2O EFs were 3.0%, 1.4%, and 1.5% for the CON, NI, and BNI treatments, respectively, with the NI and BNI treatments achieving statistically significant reductions ($P < 0.05$) of 54.5% and 49.8% relative to the CON treatment. Similarly, the 2-year mean NH_3 volatilization EFs were significantly reduced by 20.0% and 20.2% for the NI and BNI treatments, respectively, relative to the CON treatment ($P < 0.05$).

Tea rows and inter-row ridges exhibited distinct contributions to the total gaseous N emissions, with tea rows identified as the dominant emission source (Fig. 3). In the CK treatment, tea rows accounted for 46.7% of the total N_2O emissions. Inter-row ridges accounted for the remaining 53.3% (Fig. 3a). For the CON treatment, tea rows accounted for 83.1% of total N_2O emissions, whereas inter-row ridges contributed only 16.9%, with tea rows contributing 4.9-fold higher than inter-row ridges. For the NI and BNI treatments, tea rows accounted for 59.7% and 68.1% of total N_2O emissions, with corresponding proportions of 40.3% and 31.9% for inter-row ridges. In the CK treatment, tea rows accounted for 57.6% of the total NH_3 volatilization. Inter-row ridges accounted for the remaining 42.4% (Fig. 3b). For the CON treatment, NH_3 volatilization from tea rows was 2.2-fold higher than that from inter-row ridges; tea rows accounted for 68.4% of the total, and inter-row ridges for 31.6%. For the NI and BNI treatments, the proportions of total NH_3 volatilization derived from tea rows were 69.6% and 70.9%, respectively, with only a marginal difference between the two treatments (30.4% and 29.1%, respectively).

3.3 Soil physical and chemical as well as microbiological properties

Across the entire 2-year experimental period, soil available N and carbon contents in tea rows were significantly affected by both the NI and BNI treatments ($P < 0.05$) (Table S4). In the first experimental year, immediately after the combined application of chemical and organic fertilizers, all N-fertilizer treatments resulted in significantly elevated soil NH_4^+–N concentrations in tea rows compared with the CK treatment (Fig. 4a). The soil NH_4^+–N content in the short term after urea and inhibitor applications (NH_4^+–SH) was determined as the average soil NH_4^+–N content monitored from May to July 2022 within 2 months after the first fertilization of this study. Compared with the CON treatment, the NI and BNI treatments significantly reduced soil NH_4^+–SH content by 45.7% and 44.1%, respectively ($P < 0.05$) (Table S4). The results from our supplementary laboratory incubation experiment demonstrated that soil NH_4^+–N concentrations in the urea treatment (urea only) were consistently higher than those in UNI (urea + DMPP), UUI (urea + NBPT) and UUNI (urea + NBPT + DMPP) treatments throughout the incubation period, with the highest concentrations observed on day 7. In contrast, soil NH_4^+–N concentrations in the UUNI treatment remained consistently low on both day

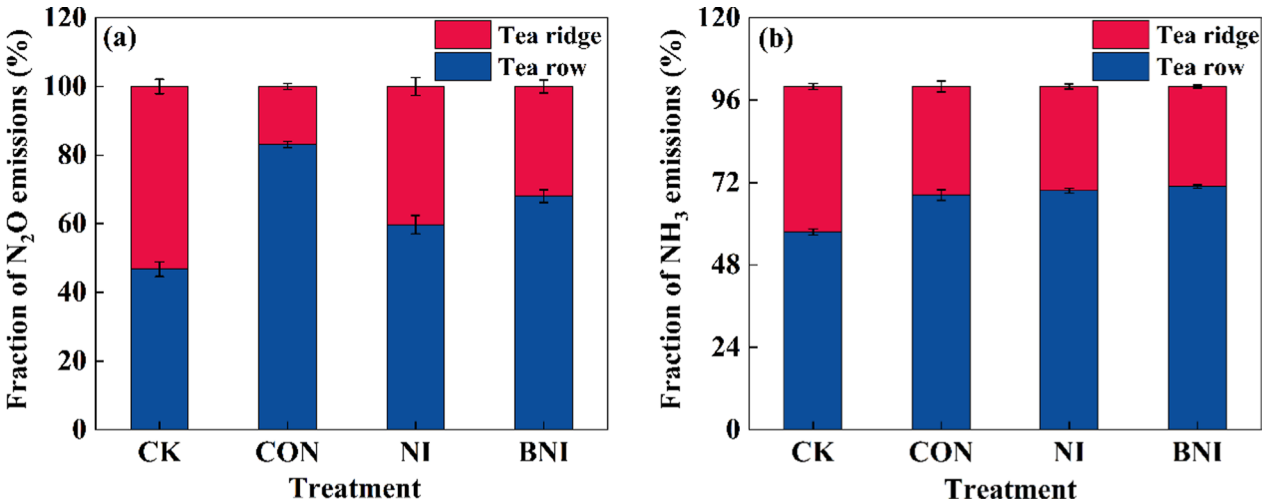

Fig. 3 Fractions of N_2O (**a**) and NH_3 (**b**) cumulative emissions from tea rows and inter-row ridges across treatments during the 2022–2024 growing season. **a** N_2O; **b** NH_3. The treatments were CK (blank control), CON (conventional fertilization), NI (dual inhibitor treatment), and BNI (biochar combined with dual inhibitor treatment). Error bars represent the standard error of three replicates ($n = 3$)

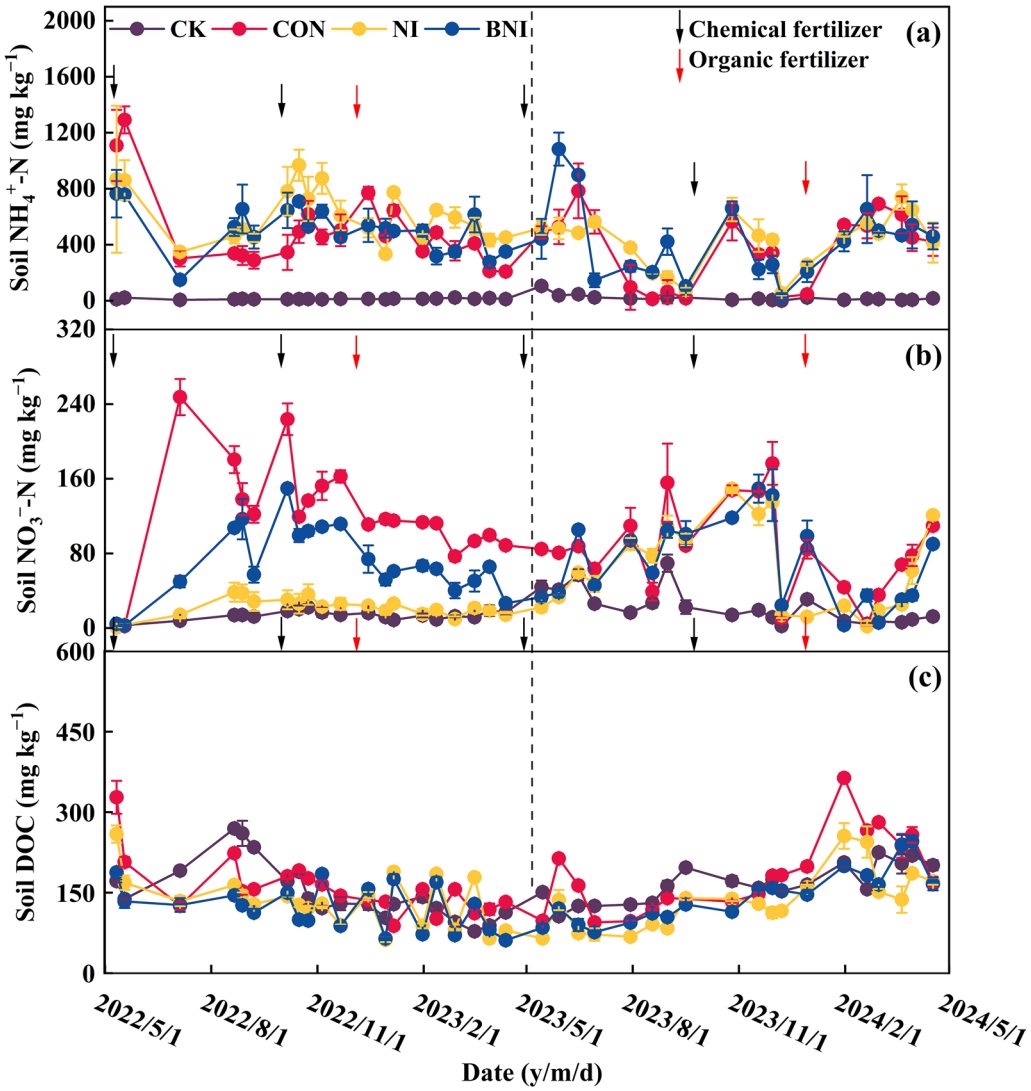

Fig. 4 Daily dynamics of soil ammonium (NH_4^+–N) (**a**), soil nitrate (NO_3^-–N) (**b**), and dissolved organic carbon (DOC) contents (**c**) across treatments in the tea plantation. The treatments were CK (blank control), CON (conventional fertilization), NI (dual inhibitors treatment), and BNI (biochar combined with dual inhibitors treatment). Arrows indicate the timing of fertilizer application. Black arrows indicate the application of chemical fertilizer, while red arrows indicate the application of rapeseed cake fertilizer. Error bars represent the standard error of three replicates ($n = 3$)

4 and day 7, whereas those in the UUI treatment began to increase by day 7 (Fig. S1a). The urea treatment resulted in significantly higher soil pH values than the UUI, UNI, and UUNI treatments on days 1 and 4. On day 7, the UNI treatment reached a relatively high pH, whereas the pH of the UUI treatment decreased to a relatively low level (Fig. S1b).

Soil NH_4^+–N concentrations were significantly higher in the first experimental year than in the second year across all treatments. In the second experimental year, the NI and BNI treatments significantly increased soil NH_4^+–N concentrations by 13.2% and 11.8%, respectively, relative to the CON treatment ($P < 0.05$). Over the 2-year period, mean soil NH_4^+–N concentrations significantly increased by 16.4% and 6.3% under the NI and BNI treatments, respectively, relative to the CON treatment ($P < 0.05$).

The temporal dynamics of soil NO_3^-–N concentrations in tea rows were consistent across the 2 experimental years (Fig. 4b). In the first experimental year, the soil NO_3^-–N concentrations in the NI and BNI treatments were reduced by 82.1% and 41.5%, respectively. In the second experimental year, the soil NO_3^-–N concentrations in the NI and BNI treatments decreased by 24.4% and 18.5%, respectively. Over the 2-year period, mean soil NO_3^-–N concentrations significantly decreased by 59.0%

and 31.5% under the NI and BNI treatments, respectively, relative to the CON treatment ($P < 0.05$).

Across the entire 2-year experimental period, no notable increase in soil DOC concentration was observed, except in the winter of the second experimental year following the incorporation of organic fertilizer into tea row soils (Fig. 4c). Soil DOC concentrations in the CON treatment were consistently higher than those in the NI and BNI treatments in both years. Specifically, soil DOC concentrations in the CON treatment were 18.7% and 30.8% higher than those in the NI and BNI treatments, respectively, in the first experimental year and 37.5% and 27.2% higher than those in the two treatments, respectively, in the second experimental year (Table S4).

Overall, the application of inhibitors differentially inhibited the abundance of genes associated with nitrification and denitrification. The abundance of AOA genes showed no significant seasonal variation (spring, summer, autumn, and winter) during the experimental period (Fig. 5a). However, in spring, the BNI treatment decreased AOA gene abundance by 15.5% relative to the CON treatment ($P < 0.05$). AOB gene abundance exhibited distinct seasonal dynamics (Fig. 5b). Compared with the CON treatment, the NI treatment reduced AOB gene abundance by 40.1%, 66.2%, 32.9%, and 11.4% in spring, summer, autumn, and winter, respectively. The BNI treatment decreased AOB gene abundance by 28.2% and 40.5% in autumn and winter, respectively, relative to the CON treatment. On average, the NI and BNI treatments significantly reduced AOB gene abundance by 39.4% and 16.0%, respectively, relative to the CON treatment ($P < 0.05$).

Neither NI nor BNI treatments significantly reduced the abundance of the denitrification functional gene *nirK* (Fig. 5c) ($P > 0.05$). Compared with the CON treatment, the NI treatment decreased the abundance of the *nirS* gene by 30.0% and 25.2% in autumn and winter, respectively (Fig. 5d). In contrast, the BNI treatment significantly reduced *nirS* abundance by 37.5% and 32.8% in spring and summer, respectively ($P < 0.05$). On average, *nirS* abundance in the NI and BNI treatments was 19.0% and 20.3% lower, respectively, than that in the CON treatment. The abundance pattern of *nosZ* was similar to that of *nirS* (Fig. 5e). In summer, *nosZ* abundance in the NI and BNI treatments decreased by 30.6% and 16.9%, respectively, compared with that in CON. The NI treatment further reduced *nosZ* abundance by 25.1% in autumn compared with the CON treatment. The BNI treatment significantly suppressed *nosZ* abundance by 40.7% in spring and by 4.2% in winter ($P < 0.05$). The average *nosZ* abundance was reduced by 16.5% and 11.7% in the NI and BNI treatments, respectively, compared with that in CON.

3.4 Crop yield, N absorption, and cumulative emissions per unit yield

Over the 2-year tea cultivation period, all N-fertilizer treatments enhanced tea yield and plant N uptake, with the BNI treatment showing the greatest effects. In the first year, the tea yield was significantly higher under the NI, BNI, and CON treatments than under the CK treatment (Fig. 6a). Tea yields for the CK, CON, NI, and BNI treatments were 5103.5, 5994.7, 5754.3, and 5933.6 kg ha^{-1}, respectively. In the second year, relative to the CK treatment, the NI, BNI, and CON treatments increased the tea yield by 13.5%, 28.2%, and 10.8%, respectively (Fig. 6b). Notably, the BNI treatment produced a 13.6% higher yield than the CON treatment ($P < 0.05$). Over the 2 years, the total yields for the NI, BNI, and CON treatments were 13.1%, 22.6%, and 14.9% higher, respectively, than those of the CK treatment ($P < 0.05$). Relative to the CON treatment, the BNI treatment increased the yield by 6.7% ($P < 0.05$; Fig. 6c). In the first year, plant N uptake in the BNI treatment was significantly enhanced by 13.0% relative to that in the CON treatment ($P < 0.05$; Fig. 6d). In the second year, the NI and BNI treatments increased plant N uptake by 12.3% and 16.0%, respectively (Fig. 6e). Over the 2 years, cumulative plant N uptake was 219.7, 245.7, 259.6, and 281.1 kg N ha^{-1} for the CK, CON, NI, and BNI treatments, respectively (Fig. 6f). Relative to the CK treatment, the NI and BNI treatments increased plant N uptake by 18.2% and 28.0%, respectively ($P < 0.05$). Relative to the CON treatment, the corresponding increases were 5.7% and 14.4%, respectively.

Yield-scaled total N_2O emissions were 1.9, 5.4, 2.9, and 3.3 kg t^{-1} for the CK, CON, NI, and BNI treatments, respectively (Fig. 6g). Compared with the CON treatment, emissions from the NI and BNI treatments were reduced by 46.1% and 38.5%, respectively ($P < 0.05$). Yield-scaled NH_3 emissions for the CK, CON, NI, and BNI treatments were 6.5, 15.8, 11.5, and 12.9 kg t^{-1}, respectively (Fig. 6h). Relative to the CON treatment, decreases of 27.0% and 18.4% were observed in the NI and BNI treatments, respectively ($P < 0.05$).

3.5 Mitigation effects and mitigation potential of N_2O and NH_3 emissions

The relationship between cumulative N_2O and NH_3 emissions was investigated in tea plantations that experience gaseous N loss during the growing season (Fig. 7a). A significant positive correlation ($R^2 = 0.8$, $P < 0.001$) was detected between N_2O and NH_3 emissions across the three fertilizer-amended treatments (CON, NI, and BNI). Compared with the CON treatment, the BNI treatment significantly reduced both N_2O and NH_3 emissions, but its overall mitigation efficacy was lower than that of the NI treatment. The CON

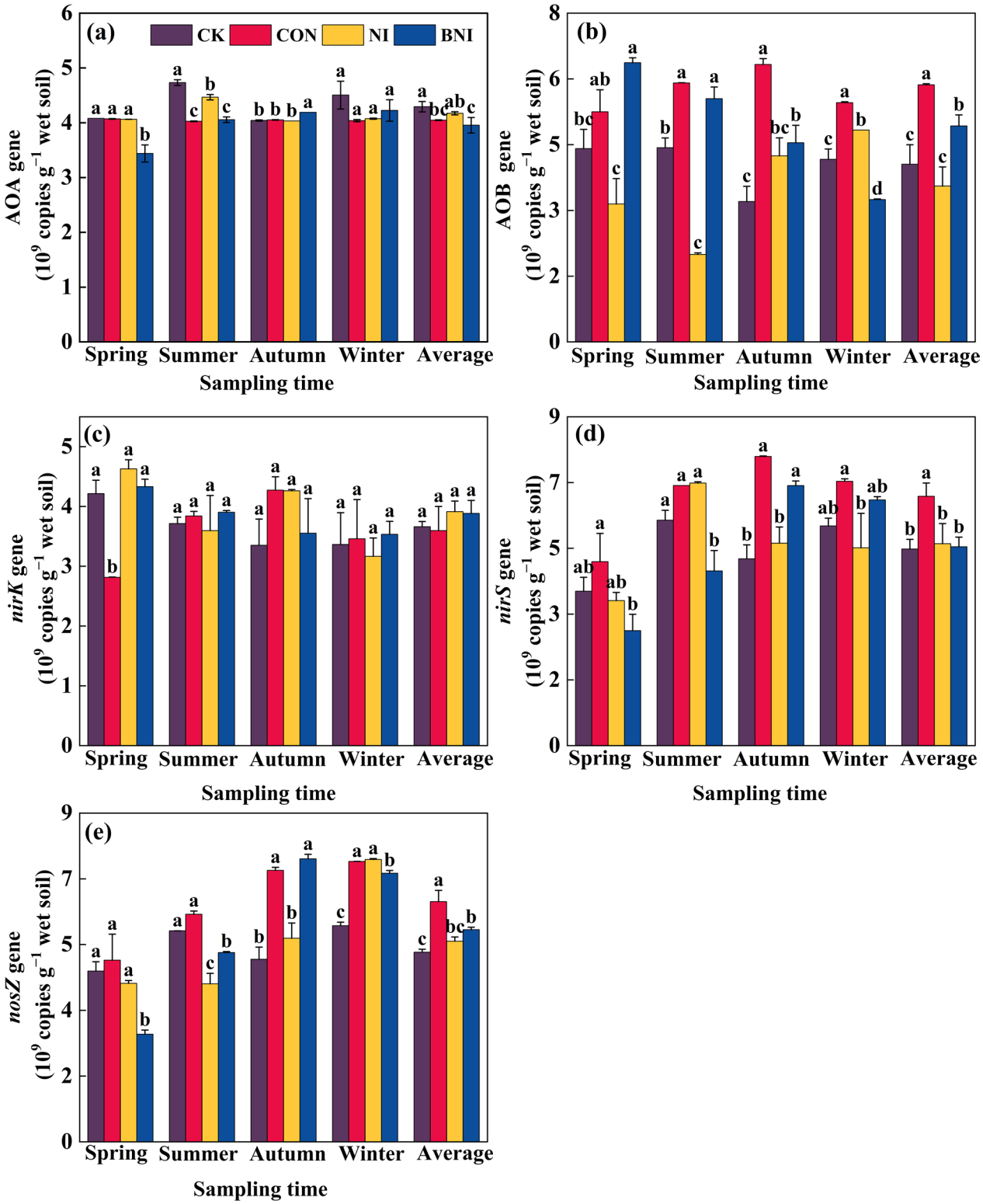

Fig. 5 Gene abundances of ammonia-oxidizing archaea (AOA) (**a**), ammonia-oxidizing bacteria (AOB) (**b**), and denitrification genes *nirK* (**c**), *nirS* (**d**), and *nosZ* (**e**) across treatments. The treatments were CK (blank control), CON (conventional fertilization), NI (dual inhibitors treatment), and BNI (biochar combined with dual inhibitors treatment). Gene abundances were measured seasonally (spring, summer, autumn, and winter) during the 2022–2023 experimental period. Averages represent seasonal means. Error bars represent the standard error of three replicates ($n = 3$). Different lowercase letters indicate significant differences among treatments within the same season at $P < 0.05$

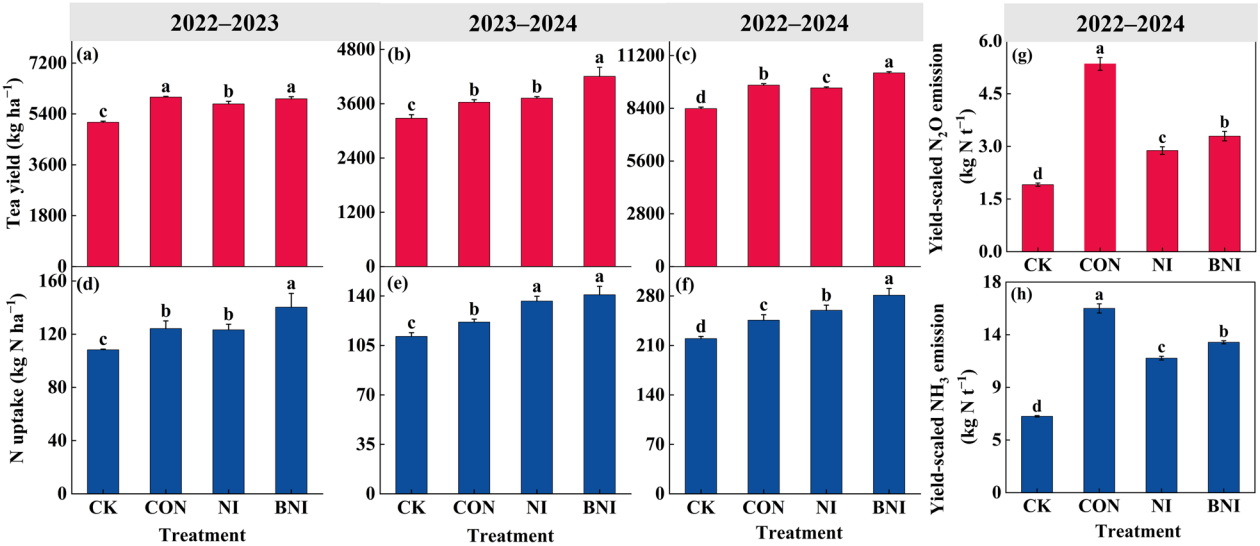

Fig. 6 Tea yield (**a**–**c**), N uptake (**d**–**f**), and yield-scaled N_2O (**g**) and NH_3 (**h**) emissions over the 2-year growing period. The treatments were CK (blank control), CON (conventional fertilization), NI (dual inhibitors treatment), and BNI (biochar combined with dual inhibitors treatment). Error bars represent the standard error of three replicates ($n = 3$). Different lowercase letters within each subfigure indicate significant differences at the $P < 0.05$ level

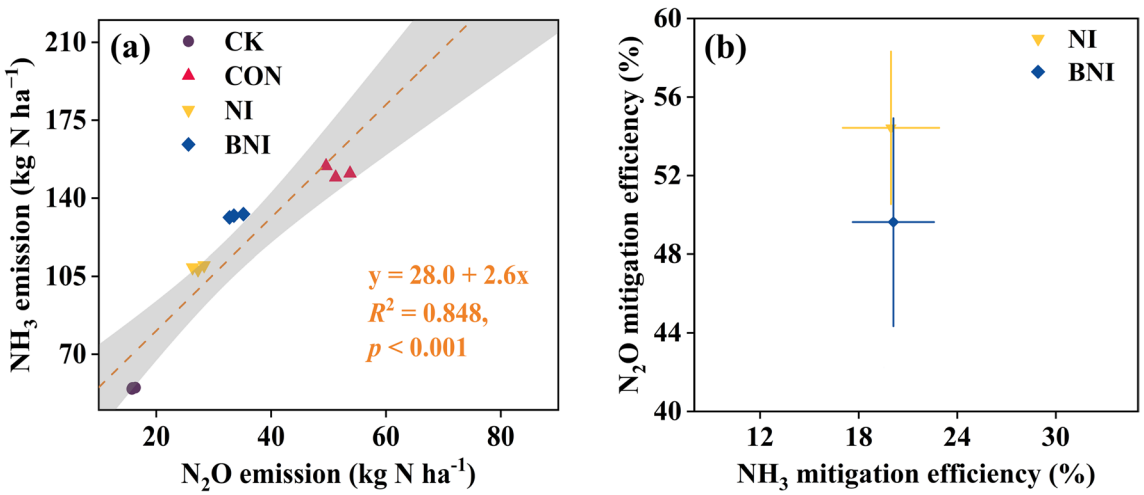

Fig. 7 Relationship between cumulative N_2O and NH_3 emissions across treatments during the 2-year experimental period (**a**), and mitigation efficiency by the dual inhibitor (NI) and by biochar combined with the dual inhibitor (BNI) (**b**). The treatments were CK (blank control), CON (conventional fertilization), NI (dual inhibitor treatment), and BNI (biochar combined with dual inhibitor treatment). The red line in panel **a** represents the linear regression across all treatments. R^2 and P values denote the coefficient of determination and the significance level of the regression, respectively. Error bars represent the standard error of three replicates ($n = 3$)

treatment posed the highest risk of combined N_2O and NH_3 loss. Furthermore, NI treatment consistently suppressed N_2O and NH_3 emissions. Compared with the CON treatment, the NI treatment demonstrated an N_2O reduction potential of 50.0–57.3% (Fig. 7b), effectively reducing emissions over the 2 years. The potential to reduce NH_3 emissions ranged from 16.7 to 22.3% (Fig. 7b). The BNI treatment reduced N_2O and NH_3 emissions by 45.5–55.6% and 17.5–22.4%, respectively, consistent with its lower efficacy compared with the NI treatment. In summary, both mitigation strategies demonstrated the potential to reduce N_2O and NH_3 emissions from tea plantations synergistically.

3.6 The impact of different environmental factors on N_2O and NH_3 emissions

SEM was employed to explore the relationships among DMPP + NBPT + BC addition, environmental factors (soil temperature, ST; soil moisture, SM), the combined abundance of ammonia-oxidizing archaea and bacteria (AOA + AOB), NH_4^+ and NO_3^- concentrations, the abundances of denitrifying bacteria (*nirS*/*nirK*), and N_2O emissions (Fig. 8a). No significant effect of *nosZ* abundance on N_2O emissions was observed. The addition of DMPP + NBPT + BC suppressed N_2O emissions primarily through two distinct mechanisms. First, it markedly inhibited the activities of AOA + AOB, thereby limiting nitrification-driven N_2O production. Second, it reduced the abundance of *nirS*/*nirK*, directly restricting denitrification. Importantly, although the application of these inhibitors induced a modest accumulation of soil NH_4^+, this increase did not translate into enhanced N_2O emissions due to the robust suppression of ammonia-oxidizing activity. Environmental variables also exerted profound direct effects on N_2O dynamics. Both ST and SM were significantly positively correlated with N_2O fluxes ($P < 0.05$). Furthermore, ST facilitated NO_3^- accumulation, thereby indirectly modulating substrate availability for denitrification. Based on the standardized total effects, N_2O emissions were negatively influenced by the addition of DMPP + NBPT + BC. In contrast, NH_4^+ content, AOA + AOB activity, soil NO_3^- content, SM, the abundances of *nirS*/*nirK*, and ST were positively associated with N_2O emissions (Fig. 8b).

SEM was also employed to analyze the effects of the DMPP + NBPT + BC addition, SM, ST, and NH_4^+–SH (early-stage soil NH_4^+–N in the field experiment) on NH_3 emissions. DMPP + NBPT + BC and ST had

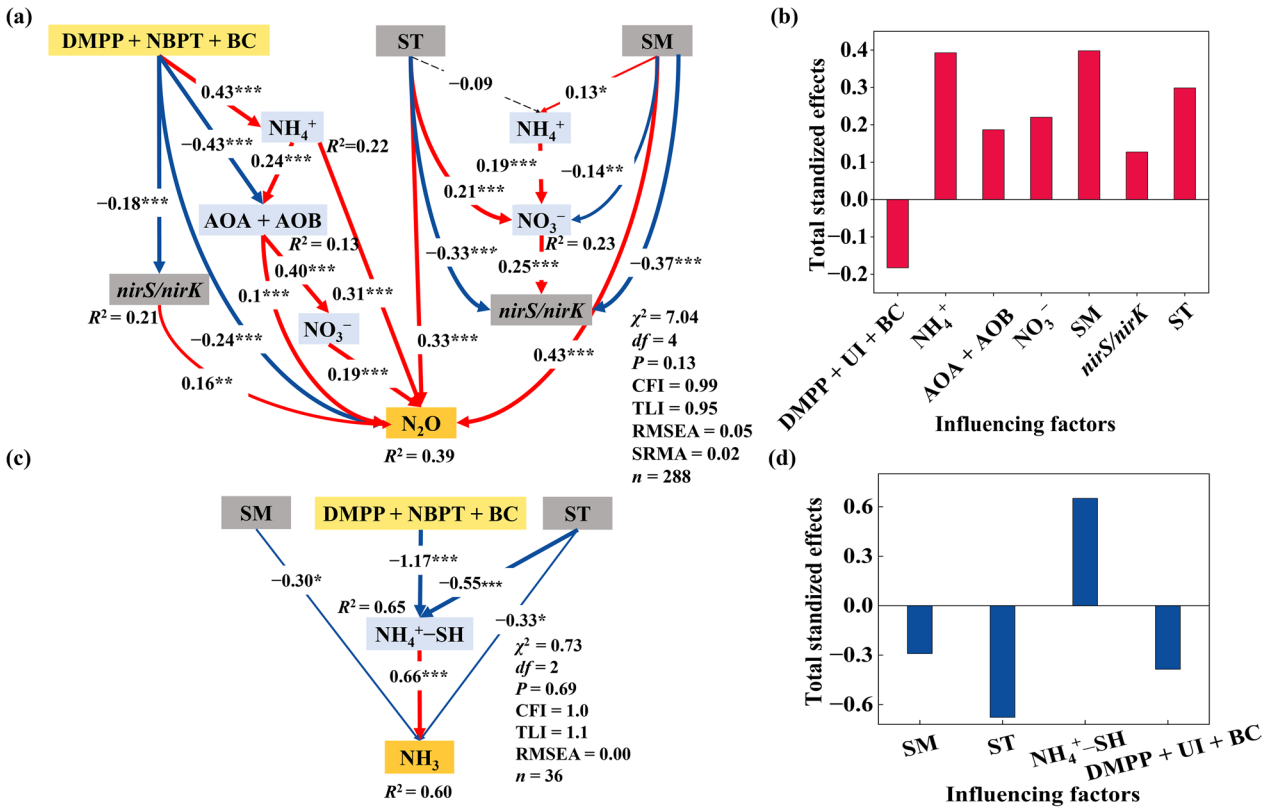

Fig. 8 Structural equation model (SEM) of the standardized total contributions of DMPP + NBPT + BC addition (combined application of DMPP, NBPT, and biochar as a categorical variable; 0 = without, 1 = with), environmental factors, soil temperature (ST), soil moisture (SM), soil properties (NO_3^-–N, NH_4^+–N), ammonia-oxidizing archaea and bacteria (AOA + AOB), and denitrifying bacteria (*nirS*/*nirK*) to N_2O emissions during 2022–2024 (**a**). * $P < 0.05$, ** $P < 0.01$, *** $P < 0.001$. Numbers adjacent to arrows are standardized path coefficients; with arrow width proportional to coefficient strength; red arrows indicate significant positive correlations, blue arrows denote significant negative correlations, and gray arrows represent non-significant paths. R^2 values represent the variance explained for each variable; *n* denotes sample size. Model fit was assessed using the comparative fit index (CFI), Tucker–Lewis index (TLI), root mean square error of approximation (RMSEA), standardized root mean square residual (SRMR), and the chi-square (χ^2) test with degrees of freedom (*df*) and its associated *P* value. The standardized total effects of DMPP + NBPT + BC, NH_4^+, AOA + AOB, NO_3^-, SM, *nirS*/*nirK* and ST on N_2O emissions (**b**). SEM for the standardized total contributions of DMPP + NBPT + BC addition, ST, SM, and NH_4^+–SH (early-stage soil NH_4^+–N in the field experiment) to NH_3 emissions, based on monthly mean values collected from May to July 2022 (**c**). The total standardized effects of DMPP + NBPT + BC, SM, ST, and NH_4^+–SH on NH_3 emissions (**d**)

highly significant negative effects on NH_4^+–SH levels ($P < 0.001$). ST and SM showed significant negative correlations with NH_3 emissions, whereas NH_4^+–SH had a highly significant positive effect on NH_3 emissions (Fig. 8c). In terms of standardized total effects, SM, ST, and DMPP + NBPT + BC amendment significantly inhibited NH_3 emissions, while NH_4^+–SH significantly promoted NH_3 emissions (Fig. 8d).

RF modeling was used to assess the effects of DMPP + NBPT + BC, AOA + AOB, *nirS*/*nirK* and soil parameters (NH_4^+–N, NO_3^-–N, temperature, and moisture) on N_2O and NH_3 emission fluxes. RF analysis showed that soil NO_3^-–N, moisture, NH_4^+–N, AOA + AOB, temperature, DMPP + NBPT + BC, and *nirS*/*nirK* were the primary drivers of N_2O emission fluxes (Fig. 9a). In contrast, the key variables associated with NH_3 volatilization included soil NH_4^+–SH, temperature, DMPP + NBPT + BC and moisture (Fig. 9b). Among these, soil NH_4^+–SH and temperature were the two most important contributors.

3.7 Net environmental economic benefit

During the 2022–2024 trial period, the NEEB was 103,749.6, 49,134.7, 100,510.8, and 116,301.8 CNY ha^{-1} yr^{-1} for the CK, CON, NI, and BNI treatments, respectively (Table 1). Compared with CON, CK, NI and BNI treatments increased NEEB by 111.2%, 104.6%, and 136.7%, respectively ($P < 0.05$). Furthermore, the NEEB under the BNI treatment was 15.7% higher than that under the NI treatment ($P < 0.05$). Therefore, both NI and BNI treatments are effective strategies for reducing gaseous N losses and enhancing yield in subtropical tea plantations, with BNI offering superior overall benefit.

4 Discussion

4.1 Mitigation of N_2O emissions by dual inhibitors and biochar

Relative to the CON treatment, cumulative N_2O emissions in the NI treatment were reduced by 47.0%, consistent with Ren et al. (2023). Additionally, the results of this study support that the NI treatment decreased AOB gene abundance by 39.4% and NO_3^-–N content by 59.0%, further substantiating the efficacy of the dual inhibitor in regulating the conversion of NH_4^+–N to NO_2^-–N and NO_3^-–N (He et al. 2022). Xia et al. (2017) reported that UIs could reduce N_2O emissions by 31%. This reduction was primarily attributed to the UIs' inhibition of urea hydrolysis, which reduces NH_4^+ availability for nitrification and thereby reduces N_2O production. A meta-analysis indicated that biochar application reduced N_2O emissions from agricultural soils by an average of 32–38% (Liu et al. 2018; Borchard et al. 2019). In this study, N_2O emissions in the BNI treatment were reduced by 34.3% relative to the CON treatment, falling within the range reported above. However, Shen et al. (2014) reported a 13–82% increase in N_2O emissions from paddy fields following the addition of biochar. Previous studies have attributed the stimulation of N_2O emissions by biochar to enhanced denitrification driven by labile organic carbon derived from biochar addition (Troy et al. 2013).

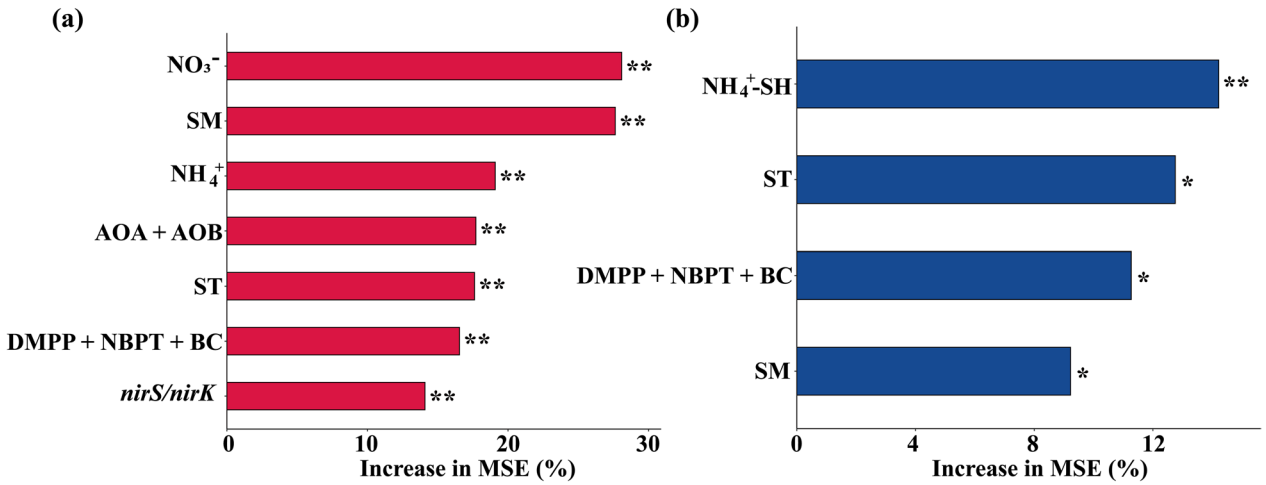

Fig. 9 Relative importance of soil environmental and climatic factors driving N_2O (**a**) and NH_3 (**b**) emissions, as determined by Random Forest modeling during the 2022–2024 tea growing season. ST, soil temperature; SM, soil moisture; NO_3^-–N, soil nitrate; NH_4^+–N, soil ammonium; NH_4^+–SH, early-stage soil NH_4^+–N; AOA + AOB, ammonia-oxidizing archaea and bacteria; *nirS/nirK*, denitrifying bacteria carrying nitrite reductase genes; DMPP + NBPT + BC, combined application of DMPP, NBPT, and biochar as a categorical variable (0 = without, 1 = with). * and ** indicate significant contributions at $P < 0.05$ and $P < 0.01$, respectively

Nevertheless, this mechanism may not apply to the present study.

This study elucidated a potential mechanism: the targeted modulation of soil microbes involved in N transformation, achieved by co-applying biochar with DMPP and NBPT, was the key driver of N_2O emission mitigation observed in the BNI treatment. Owing to its high substrate affinity, DMPP selectively binds to the active sites of ammonia monooxygenase, preferentially suppressing the growth and activity of AOB (Bachtsevani et al. 2021). This finding aligns with the 39.4% reduction in AOB gene abundance observed in the NI treatment: DMPP targeted the initial nitrification step, altered N transformation kinetics, and reduced the availability of NO_3^-–N, a key substrate for denitrification-derived N_2O production. Meanwhile, NBPT inhibited the functional expression of ureolytic microbes, slowed urea hydrolysis (Xia et al. 2017), modulated NH_4^+–N turnover dynamics, and indirectly constrained the excessive proliferation of nitrifying microbes. Biochar reshapes the community structure of N-transforming microbes by providing labile organic carbon and optimizing the soil microenvironment, thereby facilitating the enrichment of N_2O-reducing microbes harboring the *nosZ* gene while suppressing the activity of N_2O-producing microbes carrying the *nirS* and *nirK* genes (Liu et al. 2018; Borchard et al. 2019). This microbial shift provides a mechanistic basis for the complete denitrification of NO_3^- to N_2. In addition, the abundance of the denitrification gene *nirS* was significantly reduced by 20.3% (Fig. 5d), providing further evidence for the N_2O inhibition observed in the BNI treatment. Notably, the NI and BNI treatments reduced the abundance of the *nosZ* gene by 16.5% and 11.7%, respectively (Fig. 5e), which ultimately resulted in a net reduction in N_2O. This apparent discrepancy can be attributed to the distinct functional roles of the two genes: *nirS* catalyzes the reduction of NO_2^-–N to N_2O, and its decreased abundance directly curtails N_2O production. In contrast, the *nosZ* gene facilitates the further reduction of N_2O to N_2; its reduced abundance might theoretically attenuate N_2O consumption. Therefore, the suppression of *nirS* by NI and BNI treatments substantially outweighed any adverse effects resulting from the associated reduction in *nosZ* gene abundance.

The SEM revealed that DMPP + NBPT + BC significantly inhibited the activities of AOA + AOB and *nirS*/*nirK*, whereas AOA + AOB activity promoted NO_3^- production during nitrification. Furthermore, a significant positive correlation was observed between the combined abundance of AOA + AOB and soil NO_3^-–N concentration. Given that NO_3^- significantly increased N_2O emissions, DMPP + NBPT + BC likely mitigated N_2O emissions indirectly (Fig. 8a). The RF model identified soil NO_3^-–N as the dominant factor influencing N_2O emissions, thereby supporting the role of DMPP + NBPT + BC in N_2O mitigation (Fig. 8e). Thus, the SEM elucidated the mechanism by which soil NO_3^-–N, a key product of nitrification and a central substrate, drives N_2O emissions. In parallel, the RF model quantitatively clarified the dominant importance of NO_3^-–N among the environmental drivers. The two approaches provided complementary verification, jointly corroborating inferences about N_2O mitigation pathways and thereby offsetting the limitations inherent in relying on a single method.

4.2 Mitigation of NH_3 emissions by dual inhibitors and biochar

The application of UIs and NIs has been widely reported to reduce NH_3 emissions by 9–78% in intensive agricultural systems (Zaman et al. 2009). This mitigation effect is commonly attributed to the delayed urea hydrolysis induced by UIs, which decouples the simultaneous surge of NH_4^+ accumulation and microsite pH elevation, two key prerequisites for substantial NH_3 volatilization (Abdo et al. 2022). To capture the early-stage substrate availability for NH_3 volatilization, we defined NH_4^+–SH as the average soil NH_4^+–N concentration measured during May–July 2022, i.e., within 2 months after the first fertilizer application. Compared with the CON treatment, the NI and BNI treatments significantly reduced NH_4^+–SH by 45.7% and 44.1%, respectively ($P < 0.05$; Table S4). This substantial reduction in the early-stage NH_4^+–N pool directly limited the substrate available for NH_3 volatilization during the critical post-fertilization window, a period during which more than 90% of cumulative NH_3 emissions occurred in this acidic tea plantation soil. Consistent with this phenomenon, the NI and BNI treatments in this study exhibited reductions of 28.1% and 12.9% in the cumulative NH_3 emissions, respectively, relative to the CON treatment. Notably, under the NI and BNI treatments, the growing-season average soil NH_4^+–N content did not decrease; instead, it increased by 16.4% and 6.3%, respectively. This phenomenon may be related to the temporal specificity of NH_3 volatilization in acidic tea plantation soils and to the kinetic regulation of urea hydrolysis by inhibitors. Our supplementary laboratory incubation experiment directly verified this pattern: during the incubation period, in the Urea treatment, urea was rapidly hydrolyzed at the early stage, producing a large amount of NH_4^+–N and a sharp increase in soil pH; in contrast, in the UUI and UUNI treatments, both NH_4^+–N content and soil pH were significantly reduced (Fig. S1a, b), a finding that has been widely confirmed (Zhou 2017) and that served as the core driver of the significant reduction in NH_3

volatilization during the critical fertilization window in this study. After this critical window, soil pH quickly returned to its acidic background level. Even when the growing-season average soil NH_4^+–N content increased, the low-pH environment failed to provide sufficient hydroxyl groups to drive further NH_3 volatilization; notably, in the present BNI treatment, NBPT application also attenuated the elevation of soil pH following urea application, thereby enabling effective NH_3 mitigation despite the elevated soil NH_4^+–N pool. Therefore, the contribution of this retained NH_4^+–N to total cumulative emissions was negligible. Importantly, the phenomenon of reduced NH_3 emissions accompanied by increased soil NH_4^+–N content has also been widely reported in previous peer-reviewed studies (Gao et al. 2023; Abdo et al. 2022), further confirming the generality and robustness of the mechanism proposed in this study. Consistent with our results, He et al. (2018) reported that the combined application of biochar and dual inhibitors reduced NH_3 emissions by 19.8% relative to conventional fertilization, and that this mitigation effect was mainly attributed to the delayed urea hydrolysis induced by NBPT and to the adsorption of free NH_4^+ by biochar during the critical volatilization window.

In this study, the BNI treatment reduced NH_3 emissions by 12.9% relative to CON, and its mitigation efficacy improved in the second year compared with the first (Table 1); this enhanced long-term stability is attributed to biochar aging. After incorporation into the soil, biochar gradually oxidizes, significantly increasing the abundance of oxygen-containing functional groups (e.g., carboxyl [-COOH] and hydroxyl [-OH]) on its surface (Wang et al. 2020). These functional groups enhance the electrostatic adsorption of NH_4^+ during the critical volatilization window, thereby further reducing the substrate for NH_3 emissions while promoting the fixation and slow release of NH_4^+ during the non-volatilization period.

Notably, a negative correlation between NH_3 volatilization and ST was identified using SEM (Fig. 8c). This phenomenon can be attributed to the dominant role of fertilization events in governing the seasonal dynamics of NH_3 volatilization (Zhang et al. 2022). In the present study, fertilizer application in early May rapidly elevated soil NH_4^+–N concentrations, thereby driving the relatively high NH_3 fluxes recorded during the monitoring period. During the subsequent months (May–July), although air temperatures continued to rise, no additional fertilizer was applied, and the soil NH_4^+ pool was progressively depleted through crop uptake and prior volatilization losses. Consequently, NH_3 fluxes exhibited a consistent declining trend throughout this period.

The causal pathways in the SEM were constructed based on the classical theoretical framework of soil N cycling and on prior research hypotheses. It is important to emphasize that these pathways represent a priori hypothesized causal relationships grounded in established N cycling knowledge rather than direct empirical evidence of causality. For the core variables (e.g., DMPP + NBPT + BC, NH_4^+–N, NO_3^-–N, soil moisture, and microbial functional genes), all VIF values were below 5, indicating moderate correlations among variables, the absence of severe multicollinearity, and stable path coefficient estimates. Moreover, several limitations of this study warrant consideration. First, the quantification of N_2O-related functional genes was temporally decoupled from the N_2O flux measurements, and the overall sampling frequency was restricted. Furthermore, the potential contributions of fungal nitrification and denitrification were not explicitly evaluated, which may partially explain the moderate predictive power of the SEM. Finally, regarding NH_3 volatilization, the absence of continuous monitoring for soil pH and urease activity throughout the experimental period precluded a mechanistic interpretation of NH_3 emission dynamics across the entire observation cycle. Therefore, future studies examining the long-term effects of dual inhibitors on NH_3 emissions from agricultural soils should include continuous monitoring of soil pH and urease activity throughout the observation period.

4.3 Effects of dual inhibitors combined with biochar on the simultaneous mitigation of N_2O and NH_3 emissions

The results demonstrated that, compared with the CON treatment, the NI and BNI treatments significantly reduced both N_2O and NH_3 emissions (Table 1), with no trade-off effect typically associated with single-inhibitor application (Fig. 7a). For instance, Qiao et al. (2015) reported that using NIs alone led to a 39–48% reduction in N_2O emissions but a 33–67% increase in NH_3 emissions. Zhang et al. (2022) also observed similar trade-off effects when NIs were applied alone with surface-broadcast urea, a common fertilization practice in agricultural production. This trade-off occurs because the inhibition of AOB activity induced by NIs delays the conversion of NH_4^+ to NO_2^-/NO_3^-, leading to excessive NH_4^+ accumulation in the soil and thus an elevated risk of NH_3 volatilization. The simultaneous mitigation of N_2O and NH_3 observed in this study was driven by the complementary regulation of soil N transformation by UIs and NIs. Specifically, UIs retard urea hydrolysis and reduce the substrate pool for NH_3 volatilization, whereas NIs block nitrification and weaken the primary production pathway of N_2O. This complementary regulation avoids the trade-off effect associated with a single inhibitor application, thereby achieving simultaneous reductions

in both gases. The effects of biochar on N_2O and NH_3 emissions have been widely reported to vary substantially across agroecosystems. Some studies report mitigation achieved through reduced ammonification, adsorption of NH_4^+/NO_3^-, promotion of complete denitrification, or increased soil pH (Fungo et al. 2019; Park et al. 2019; Wu et al. 2019; Zhong et al. 2025). In contrast, other studies report that biochar can increase emissions by increasing the viscosity of liquid organic fertilizer, reducing soil infiltration, or adsorbing nitrification inhibitors (Deng et al. 2019).

Notably, while the dual-inhibitor treatment alone achieved simultaneous mitigation of N_2O and NH_3, the combination of biochar and dual inhibitors further enhanced the long-term stability of this dual-gas mitigation effect. However, biochar did not increase the magnitude of N_2O mitigation compared with the NI treatment, and its primary role was to enhance the long-term stability of the mitigation effect. This outcome is attributed to the high surface area and abundant functional groups of biochar, which enable the adsorption of both NH_4^+ and inhibitor molecules. This adsorption not only reduced the availability of NH_4^+ but also slowed inhibitor release and protected the inhibitors from degradation, thereby prolonging inhibitory activity and enhancing long-term mitigation stability. He et al. (2022) reported consistent results in rice fields, where biochar combined with dual inhibitors reduced N_2O and NH_3 emissions by 14.6% and 24.3%, respectively. The underlying mechanisms were attributed to the adsorption of NH_4^+ by biochar, coupled with urease inhibitors, to mitigate NH_3 emissions, and to the targeted inhibition of AOB abundance by a nitrification inhibitor to slow nitrification and curb N_2O production. Notably, this study further demonstrated that biochar could adsorb inhibitor molecules, retard their release and degradation, and extend the effective inhibition period, which is consistent with our observation that biochar primarily enhances the long-term stability of the dual-gas mitigation effect. In our study, we quantified emission benefits, and the results indicated that both treatments showed strong potential for emission reductions. The N_2O mitigation potential of the NI treatment was slightly higher than that of the BNI treatment. However, the two treatments exhibited comparable NH_3 mitigation effects (Fig. 7b). These results suggest enhanced N retention within the soil-crop system for recycling and a significantly reduced risk of N loss through leaching and runoff. These findings were derived from field plot experiments. However, large-scale agricultural environments are heterogeneous and may exhibit uncertain long-term effects (Kravchenko et al. 2017). Therefore, economic assessments are crucial to evaluate the feasibility of large-scale adoption. Future studies should, therefore, be conducted across multiple scales, considering the key driving factors in diverse agricultural systems.

4.4 Biochar and inhibitor addition on yield and yield-scaled N_2O and NH_3 emissions

The increases in yield and plant N uptake observed in the BNI treatment are consistent with the findings of Cheng et al. (2022). This enhancement can be attributed to two synergistic mechanisms. First, as an ammonium-preferring crop, tea benefits from the enhanced retention of soil NH_4^+–N mediated by nitrification inhibitors. Second, biochar adsorbs both N and moisture from the soil (Yang et al. 2025), thereby reducing N loss and prolonging N availability within the root zone. This enhanced retention facilitates more efficient N utilization by tea plants, thereby improving yield.

Consequently, the additional cost of biochar application is economically justified, as it is offset by yield gains while concurrently providing environmental benefits through reduced N emissions. Increased rice yields with varying levels of biochar have been documented in paddy soils (Jin et al. 2024). Compared with the control, biochar addition increased the rice yield by 116.4–145.2%. However, the NI treatment did not significantly increase tea yield relative to CON; this was likely attributable to a 30% reduction in the N application rate. Nevertheless, plant N uptake was enhanced by 5.7% in the NI treatment. These findings demonstrate that optimizing N application can simultaneously stabilize yield, improve N uptake efficiency, and reduce N loss.

In contrast, Ding et al. (2015) reported that the combined application of NBPT and DCD had no significant effect on wheat yield in sandy loam soils of the North China Plain, suggesting that excessive N fertilizer application may mask or attenuate the yield-enhancing effects of inhibitors. Yield-scaled N_2O emissions can serve as an indicator of the trade-off between N_2O emissions and tea yield. In this study, both the NI and BNI treatments significantly reduced yield-scaled N_2O and NH_3 emissions, which is consistent with previous findings (He et al. 2022). Compared with the CON treatment, the NI treatment significantly lowered N_2O and NH_3 emissions without incurring a significant yield reduction. Thus, the reduction in yield-scaled emissions in the NI treatment was solely attributable to decreased gaseous emissions.

In contrast, for the BNI treatment, this reduction was driven by both increased yield and reduced N_2O and NH_3 emissions relative to the CON treatment. Consequently, the BNI treatment resulted in significant reductions in yield-scaled emissions. This study demonstrated that the application of dual inhibitors, either alone or in combination with biochar, effectively reduced yield-scaled N_2O and NH_3 emissions. These findings indicate that such

mitigation strategies can reduce gaseous N emissions without compromising the yield. This study also revealed that gaseous N emissions originate predominantly from tea rows rather than from ridges; this spatial heterogeneity can be attributed to three interacting factors: fertilizer placement, root distribution, and soil moisture gradients. First, fertilizer was predominantly banded within the tea rows, leading to significantly higher soil NH_4^+–N and NO_3^-–N availability than in the ridges. Second, the tea rows constituted the primary root zone. Abundant root exudates in this zone supply labile carbon, thereby stimulating microbial nitrification and denitrification. Third, the slightly concave microtopography of the rows facilitated rainwater retention, creating favorable conditions for gaseous N production. In contrast, the convex ridge structure restricts water accumulation and the associated microbial activity.

From an N footprint perspective, the reductions in N_2O and NH_3 emissions and in soil NO_3^-–N content achieved by the NI and BNI treatments can diminish NO_3^-–N leaching losses, as NO_3^-–N is weakly adsorbed by soil colloids and is highly susceptible to leaching. Additionally, the adsorption of NH_4^+–N by biochar can reduce runoff losses since NH_4^+–N is readily adsorbed by soil colloids, and these colloids are primarily lost via surface runoff. These combined effects act synergistically to reduce the N footprint of tea production and mitigate the risk of N pollution migrating to aquatic environments through runoff and leaching.

5 Conclusions

A 2-year field study conducted in a subtropical acidic tea plantation demonstrated that both the NI and BNI treatments significantly reduced N_2O and NH_3 emissions. Quantitative analysis revealed differences in mitigation efficacy: the NI treatment achieved slightly greater N_2O mitigation than the BNI treatment, whereas the two treatments demonstrated comparable effectiveness in reducing NH_3 emissions. Mechanistically, NBPT significantly reduced short-term soil NH_4^+–N concentrations following fertilization, thereby lowering the substrate availability for NH_3 volatilization, while DMPP significantly suppressed the abundance of key N-cycling functional genes, particularly AOB and *nirS*, thereby inhibiting nitrification-driven N_2O production. Compared with the CON treatment, the BNI treatment increased tea yield and plant N uptake. In contrast, NI treatment maintained tea yield while enhancing plant N uptake with a 30% reduction in the N application rate. Both the NI and BNI treatments increased NEEB. Future research should systematically elucidate the underlying soil N transformation processes and microbial mechanisms associated with the combined application of NBPT, DMPP, and biochar.

Supplementary Information

The online version contains supplementary material available at https://doi.org/10.1007/s42773-026-00635-7.

Additional file 1.

Acknowledgements
This study was supported by the National Natural Science Foundation of China (42161144002) and National Key Research and Development Program of China (2021YFD1700801).

Author contributions
Jianlin Shen conceived, designed, and financially supported the study; Yuefeng Li analyzed the data, wrote the paper, and conducted the analytical work with Yanyan Li, Huixiu Zhan, Haifeng Zhang, and Qiyuan Liao; Chengli Tong, Yong Li and Jinshui Wu revised the manuscript. All the authors have read and approved the final version of the manuscript.

Funding
This study was financially supported by the National Natural Science Foundation of China (42161144002) and National Key Research and Development Program of China (2021YFD1700801).

Availability of data and materials
All data generated or analyzed during this study are included in this published article (and its supplementary information files).

Declarations

Competing interests
The authors declare no competing financial interests or personal relationships that could influence the work reported in this study.

Author details
[1]Changsha Research Station for Agricultural & Environmental Monitoring, Institute of Subtropical Agriculture, Chinese Academy of Sciences, Changsha 410125, China. [2]State Key Laboratory of Atmospheric Boundary Layer Physics and Atmospheric Chemistry, Institute of Atmospheric Physics, Chinese Academy of Sciences, Beijing 100029, China.

Received: 11 November 2025 Revised: 8 May 2026 Accepted: 14 May 2026
Published online: 16 June 2026

References

Abdo AI, Xu Y, Shi D, Li J, Li H, El-Sappah AH, Elrys AS, Alharbi SA, Zhou C, Wang L, Kuzyakov Y (2022) Nitrogen transformation genes and ammonia emission from soil under biochar and urease inhibitor application. Soil till Res 223:105491

Bachtsevani E, Papazlatani C, Rousidou K, Lampronikou E, Menkissoglu-Spiroudi U, Nicol G, Karpouzas D, Papadopoulou E (2021) Effects of the nitrification inhibitor 3,4-dimethylpyrazole phosphate (DMPP) on the activity and diversity of the soil microbial community under contrasting soil pH. Biol Fertil Soils 57:1–19

Bao SD (2000) Soil and agro-chemistry analysis, 3rd ed. China Agric. Press, Beijing

Borchard N, Schirrmann M, Cayuela ML, Kammann C, Wrage-Mönnig N, Estavillo JM, Fuertes-Mendizabal T, Sigua G, Spokas K, Ippolito JA, Novak J (2019) Biochar, soil and land-use interactions that reduce nitrate leaching and N_2O emissions: a meta-analysis. Sci Total Environ 651(2):2354–2364

Cai S, Zhao X, Pittelkow CM, Fan M, Zhang X, Yan X (2023) Optimal nitrogen rate strategy for sustainable rice production in China. Nature 615:73–79

Chen D, Li Y, Wang C, Liu X, Wang Y, Shen J, Qin J, Wu J (2019a) Dynamics and underlying mechanisms of N_2O and NO emissions in response to a transient land-use conversion of Masson pine forest to tea field. Sci Total Environ 693:133549

Chen H, Yin C, Fan X, Ye M, Peng H, Li T, Zhao Y, Wakelin SA, Chu G, Liang Y (2019b) Reduction of N_2O emission by biochar and/or 3,4-dimethylpyrazole phosphate (DMPP) is closely linked to soil ammonia oxidizing bacteria and nosZI-N_2O reducer populations. Sci Total Environ 694:133658

Cheng Y, Elrys AS, Wang J, Xu C, Ni K, Zhang J, Wang S, Cai Z, Pacholski A (2022) Application of enhanced-efficiency nitrogen fertilizers reduces mineral nitrogen usage and emissions of both N_2O and NH_3 while sustaining yields in a wheat-rice rotation system. Agric Ecosyst Environ 324:107720

Cui X, Chen S, Yang J, Zhao L, Hu T, Lu J, Li A, Zhang J, Chang Z, Liu J, Wang X (2025) Ammonia volatilization and nitrous oxide emission and their responses to environmental indicators under different irrigation levels and nitrogen fertilizer synergists. J Environ Manag 377:124580

Deng B, Wang S, Xu X, Wang H, Hu D, Guo X, Shi Q, Siemann E, Zhang L (2019) Effects of biochar and dicyandiamide combination on nitrous oxide emissions from *Camellia oleifera* field soil. Environ Sci Pollut Res 26:4070–4077

Ding W, Chen Z, Yu H, Luo J, Yoo G, Xiang J, Zhang H, Yuan J (2015) Nitrous oxide emission and nitrogen use efficiency in response to nitrophosphate, *N*-(*n*-butyl) thiophosphoric triamide and dicyandiamide of a wheat cultivated soil under sub-humid monsoon conditions. Biogeosciences 12(3):803–815

Elrys AS, Uwiragiye Y, Zhang Y, Abdel-Fattah MK, Chen Z, Zhang H, Meng L, Wang J, Zhu T, Cheng Y, Zhang J, Cai Z, Chang SX, Müller C (2023) Expanding agroforestry can increase nitrate retention and mitigate the global impact of a leaky nitrogen cycle in croplands. Nat Food 4:109–121

Food and Agriculture Organization of the United Nations Website. 2018. https://www.fao.org/faostat/en/

Fungo B, Lehmann J, Kalbitz K, Thiongo M, Tenywa M, Okeyo I, Neufeldt H (2019) Ammonia and nitrous oxide emissions from a field ultisol amended with tithonia green manure, urea, and biochar. Biol Fertil Soils 55:135–148

Gao X, Yang J, Liu W, Li X, Zhang W, Wang A (2023) Effects of alkaline biochar on nitrogen transformation with fertilizer in agricultural soil. Environ Res 233:116084

Han B, Yao Y, Liu B, Wang Y, Su X, Ma L, Liu D, Niu S, Chen X, Li Z (2023a) Relative importance between nitrification and denitrification to N_2O from a global perspective. Glob Change Biol 30(1):e17082

Han X, Yu HY, Zheng NG, Ge CQ, Yao HY (2023b) Nitrous oxide emissions from tea plantations: a review. Chin J Appl Ecol 34:805–814

Hao X, Sun L, Zhou B, Ma X, Wang S, Liu S, Ji J, Kuang E, Qiu S (2023) Change in maize yield, N use efficiencies and climatic warming potential after urea combined with Nitrapyrin and NBPT during the growing season in a black soil. Soil till Res 231:105721

He T, Liu D, Yuan J, Ni K, Zaman K, Luo J, Lindsey S, Ding W (2018) A 2-year study on the combined effects of biochar and inhibitors on ammonia volatilization in an intensively managed rice field. Agric Ecosyst Environ 264:44–53

He T, Yuan J, Xiang J, Lin Y, Luo J, Lindsey S, Liao X, Liu D, Ding W (2022) Combined biochar and double inhibitor application offsets NH_3 and N_2O emissions and mitigates N leaching in paddy fields. Environ Pollut 292:118344

He D, Dong Z, Zhu B (2024) An optimal global biochar application strategy based on matching biochar and soil properties to reduce global cropland greenhouse gas emissions: findings from a global meta-analysis and density functional theory calculation. Biochar 6:92

Hu W, Zhang Y, Rong X, Zhou X, Fei J, Peng J, Luo G (2024) Biochar and organic fertilizer applications enhance soil functional microbial abundance and agroecosystem multifunctionality. Biochar 6:3

Jin F, Piao J, Miao S, Che W, Li X, Li X, Shiraiwa T, Tanaka T, Taniyoshi K, Hua S, Lan Y (2024) Long-term effects of biochar one-off application on soil physicochemical properties, salt concentration, nutrient availability, enzyme activity, and rice yield of highly saline-alkali paddy soils: based on a 6-year field experiment. Biochar 6:40

Ju X, Xing G, Chen X, Zhang S, Zhang L, Liu X, Cui Z, Yin B, Christie P, Zhu Z, Zhang F (2009) Reducing environmental risk by improving N management in intensive Chinese agricultural systems. Proc Natl Acad Sci U S A 106(9):3041–3046

Kravchenko AN, Snapp SS, Robertson GP (2017) Field-scale experiments reveal persistent yield gaps in low-input and organic cropping systems. Proc Natl Acad Sci U S A 114(5):926–931

Li HR, Song XT, Bakken LR, Ju XT (2023a) Reduction of N_2O emissions by DMPP depends on the interactions of nitrogen sources (digestate vs. urea) with soil properties. J Integr Agric 22(1):251–264

Li Z, Wang B, Liu Z, Zhang P, Yang B, Jia Z (2023b) Ridge–furrow planting with film mulching and biochar addition can enhance the spring maize yield and water and nitrogen use efficiency by promoting root growth. Field Crops Res 303:109139

Liu Q, Zhang Y, Liu B, Amonette JE, Lin Z, Liu G, Ambus P, Xie ZB (2018) How does biochar influence soil N cycle? A meta-analysis. Plant Soil 426:211–225

Ngaba MJY, Mgelwa AS, Ibrahim MM, Rennenberg H, Hu B (2026) Biochar amendments mitigate soil greenhouse gas emissions by shifted soil properties, enzyme activities, and nitrogen cycling processes. Carbon Res 5:14

Park MH, Jeong S, Kim JY (2019) Adsorption of NH_3–N onto rice straw-derived biochar. J Environ Chem Eng 7(2):103039

Pokharel P, Chang SX (2021) Biochar decreases the efficacy of the nitrification inhibitor nitrapyrin in mitigating nitrous oxide emissions at different soil moisture levels. J Environ Manage 295:113080

Qi Z, Wang M, Dong Y, He M, Dai X (2022) Effect of coated urease/nitrification inhibitor synergistic urea on maize growth and nitrogen use efficiency. J Soil Sci Plant Nutr 22:5207–5216

Qiao C, Liu L, Hu S, Compton JE, Greaver TL, Li Q (2015) How inhibiting nitrification affects nitrogen cycle and reduces environmental impacts of anthropogenic nitrogen input. Glob Change Biol 21(3):1249–1257

Ren B, Huang Z, Liu P, Zhao B, Zhang J (2023) Urea ammonium nitrate solution combined with urease and nitrification inhibitors jointly mitigate NH_3 and N_2O emissions and improves nitrogen efficiency of summer maize under fertigation. Field Crops Res 296:108909

Shen J, Tang H, Liu J, Wang C, Li Y, Ge T, Jones DL, Wu J (2014) Contrasting effects of straw and straw-derived biochar amendments on greenhouse gas emissions within double rice cropping systems. Agric Ecosyst Environ 188:264–274

Shen J, Li Y, Wang Y, Li Y, Zhu X, Jiang W, Li Y, Wu J (2022) Soil N cycling and environmental impacts in the subtropical hilly region of China: evidence from measurements and modeling. Front Agric Sci Eng 9(3):407–424

Smerald A, Kraus D, Rahimi J, Fuchs K, Kiese R, Butterbach-Bahl K, Scheer C (2023) A redistribution of nitrogen fertiliser across global croplands can help achieve food security within environmental boundaries. Commun Earth Environ 4:315

Song Y, Zhang X, Ma B, Chang SX, Gong J (2014) Biochar addition affected the dynamics of ammonia oxidizers and nitrification in microcosms of a coastal alkaline soil. Biol Fertil Soils 50:321–332

Song L, Wang A, Li Z, Kang R, Walters WW, Pan Y, Quan Z, Huang S, Fang Y (2024) Large seasonal variation in nitrogen isotopic abundances of ammonia volatilized from a cropland ecosystem and implications for regional NH_3 source partitioning. Environ Sci Technol 58(2):1177–1186

Troy SM, Lawlor PG, O'Flynn CJ, Healy MG (2013) Impact of biochar addition to soil on greenhouse gas emissions following pig manure application. Soil Biol Biochem 60:173–181

Uwiragiye Y, Wang J, Huang Y, Wu L, Zhou J, Zhang Y, Chen M, Jing H, Qian Y, Elrys AS, Cheng Y, Cai Z, Xu M, Chang SX, Müller C (2024) Global ecosystem nitrogen cycling reciprocates between land-use conversion and its reversal. Glob Change Biol 30(10):e17537

Wang C, Shen J, Liu J, Qin H, Yuan Q, Fan F, Hu Y, Wang J, Wei W, Li Y, Wu J (2019) Microbial mechanisms in the reduction of CH_4 emission from double rice cropping system amended by biochar: a 4-year study. Soil Biol Biochem 135:251–263

Wang L, O'Connor D, Rinklebe J, Ok YS, Tsang DCW, Shen Z, Hou D (2020) Biochar aging: mechanisms, physicochemical changes, assessment, and implications for field applications. Environ Sci Technol 54(23):14797–14814

Wang C, Li Z, Shen J, Li Y, Chen D, Bolan N, Li Y, Wu J (2023a) Biochar amendment increases the abundance and alters the community composition of diazotrophs in a double rice cropping system. Biol Fertil Soils 59:873–886

Wang J, Sha Z, Zhang J, Qin W, Xu W, Goulding K, Liu X (2023b) Improving nitrogen fertilizer use efficiency and minimizing losses and global

warming potential by optimizing applications and using nitrogen synergists in a maize-wheat rotation. Agric Ecosyst Environ 353:108538
Wang J, Wang B, Bian R, He W, Liu Y, Shen G, Xie H, Feng Y (2024) Bibliometric analysis of biochar-based organic fertilizers in the past 15 years: focus on ammonia volatilization and greenhouse gas emissions during composting. Environ Res 243:117853
Wang M, He P, Fan D, Jiang R, Zou G, Song D, Zhang L, Zhang Y, He W (2025) Trade-offs between agronomic and environmental benefits: a comparison of inhibitors with controlled release fertilizers in global maize systems. Field Crops Res 323:109768
Wu Y, Li Y, Fu X, Liu X, Shen J, Wang Y, Wu J (2016) Three-dimensional spatial variability in soil microorganisms of nitrification and denitrification at a row-transect scale in a tea field. Soil Biol Biochem 103:452–463
Wu Y, Li F, Zheng H, Hong M, Hu Y, Zhao B, De H (2019) Effects of three types of soil amendments on yield and soil N balance of maize-wheat rotation system in the Hetao Irrigation Area, China. J Arid Land 11:904–915
Wu Y, Li Y, Wang H, Wang Z, Fu X, Shen J, Wang Y, Liu X, Meng L, Wu J (2021) Response of N_2O emissions to biochar amendment on a tea field soil in subtropical central China: a 3-year field experiment. Agric Ecosyst Environ 318:107473
Xia L, Lam SK, Chen D, Wang J, Tang Q, Yan X (2017) Can knowledge-based N management produce more staple grain with lower greenhouse gas emission and reactive nitrogen pollution? a meta-analysis. Glob Change Biol 23(5):1917–1925
Xu Q, Yang Y, Hu K, Chen J, Djomo SN, Yang X, Knudsen MT (2021) Economic, environmental, and emergy analysis of China's green tea production. Sustain Prod Consum 28:269–280
Yang Z, Liu W, Fan X, Gao H, Xu X, Liu C, Chai Y, Zhang M, Drosos M, Shan S (2025) The molecular composition of soil organic matter is regulated by bacterial community under biochar application. Geoderma 457:117308
Yi W, Liu G, Wang M, Wang J, Chen D, Shen J (2025) Increased nitrogen deposition and airborne particulate matter pollution in the vicinity of intensive animal farms caused by ammonia emissions. Agric Ecosyst Environ 387:109634
Zaman M, Saggar S, Blennerhassett JD, Singh J (2009) Effect of urease and nitrification inhibitors on N transformation, gaseous emissions of ammonia and nitrous oxide, pasture yield and N uptake in grazed pasture system. Soil Biol Biochem 41(6):1270–1280
Zhang C, Song X, Zhang Y, Wang D, Rees RM, Ju X (2022) Using nitrification inhibitors and deep placement to tackle the trade-offs between NH_3 and N_2O emissions in global croplands. Glob Change Biol 28(14):4409–4422
Zhong L, Wang P, Gu Z, Song Y, Cai X, Yu G, Xu X, Kuzyakov Y (2025) Biochar reduces N_2O emission from fertilized cropland soils: a meta-analysis. Carbon Res 4:31
Zhou X (2017) Influence of biochemical inhibitor combination on nitrogen transformation in yellow clayey soil and its ecological environment effect. PhD dissertation, Zhejiang University
Zhu X, Shen J, Li Y, Liu X, Wu W, Zhou F, Wang J, Reis S, Wu J (2021) Nitrogen emission and deposition budget in an agricultural catchment in subtropical central China. Environ Pollut 289:117870
Zou ZH, Shen C, Li X, Zhang LP, Zhang L, Han WY, Yan P (2021) Status quo of nitrogen fertilizer application and loss in tea garden of China. Plant Nutr Fertil Sci 27:153–160